Supporting Information

Control of Reaction Pathways in the Photochemical Reaction of a Quinone with Tetramethylethylene by Metal Binding

Hiroaki Yamamoto,[a] Kei Ohkubo,[b] Seiji Akimoto,[c] Shunichi Fukuzumi[b] and Akihiko Tsuda*[a]

[a] Department of Chemistry, Graduate School of Science, Kobe University, 1-1 Rokkodai-cho, Nada-ku, Kobe 657-8501, Japan

[b] Department of Material and Life Science, Graduate School of Engineering, Osaka University, ALCA, Japan Science and Technology Agency, Suita, Osaka 565-0871, Japan

[c] Molecular Photoscience Research Center, Kobe University, 1-1 Rokkodai-cho, Nada-ku, Kobe 657-8501, Japan

Table of Contents

1. Evaluations of the binding constants of **QE_3** with metal ions s3
2. ^{1}H NMR spectroscopy for a mixture of TME and $Pd(OAc)_2$ s4
3. ^{1}H NMR spectroscopy for a ternary mixture of **QE_3**, TME, and $Pd(OAc)_2$ s5
4. Cyclic voltammetry for mixtures of **QE_3** and metal salt s6
5. HPLC traces for the photochemical reactions of **QE_n** s7
6. X-ray crystallography of **$2aE_0$** s8
7. Photodecomposition of **QE_0** s10
8. Cyclic voltammetry of TME s11
9. Phosphorescence spectra of **QE_n** in the absence or presence of metal salt. s12
10. Charge and spin densities of **$QE_3^{\bullet-}$** and **$QE_3^{\bullet-}\supset Ca(ClO_4)_2$** in DFT calculations with UB3LYP/6-31+G(d,p) s13
11. Charge and spin densities of **$QE_0^{\bullet-}$** and **$QE_0^{\bullet-}$**/$Pd(OAc)_2$ in DFT calculations with UB3PW91/LANL2DZ s14
12. Formation of 2,3-dimethyl-1,3-butadiene in the photochemical reaction s15
13. Photochemical reaction of **QE_0** with TME in the presence of $Pd(OAc)_2$ s16
14. Photochemical reaction of **QE_3** with TME in the presence of $Pd(OAc)_2$. s17
15. Photochemical reaction of **QE_3** with TME in the presence of $Pd(OAc)_2$ (continued) s18
16. Hyperfine coupling constants predicted by DFT calculations s19
17. Detection of a palladium-complex of **QE_3** generated upon photo-irradiation in ESI-FT-MS s20
18. Changes in ESR spectrum of **$QE_3^{\bullet-}$**/$TME^{\bullet+}$ upon metal binding s21
19. ^{1}H and ^{13}C NMR spectra of products s22
20. References s33

1. Evaluations of the binding constants of QE_3 with metal ions

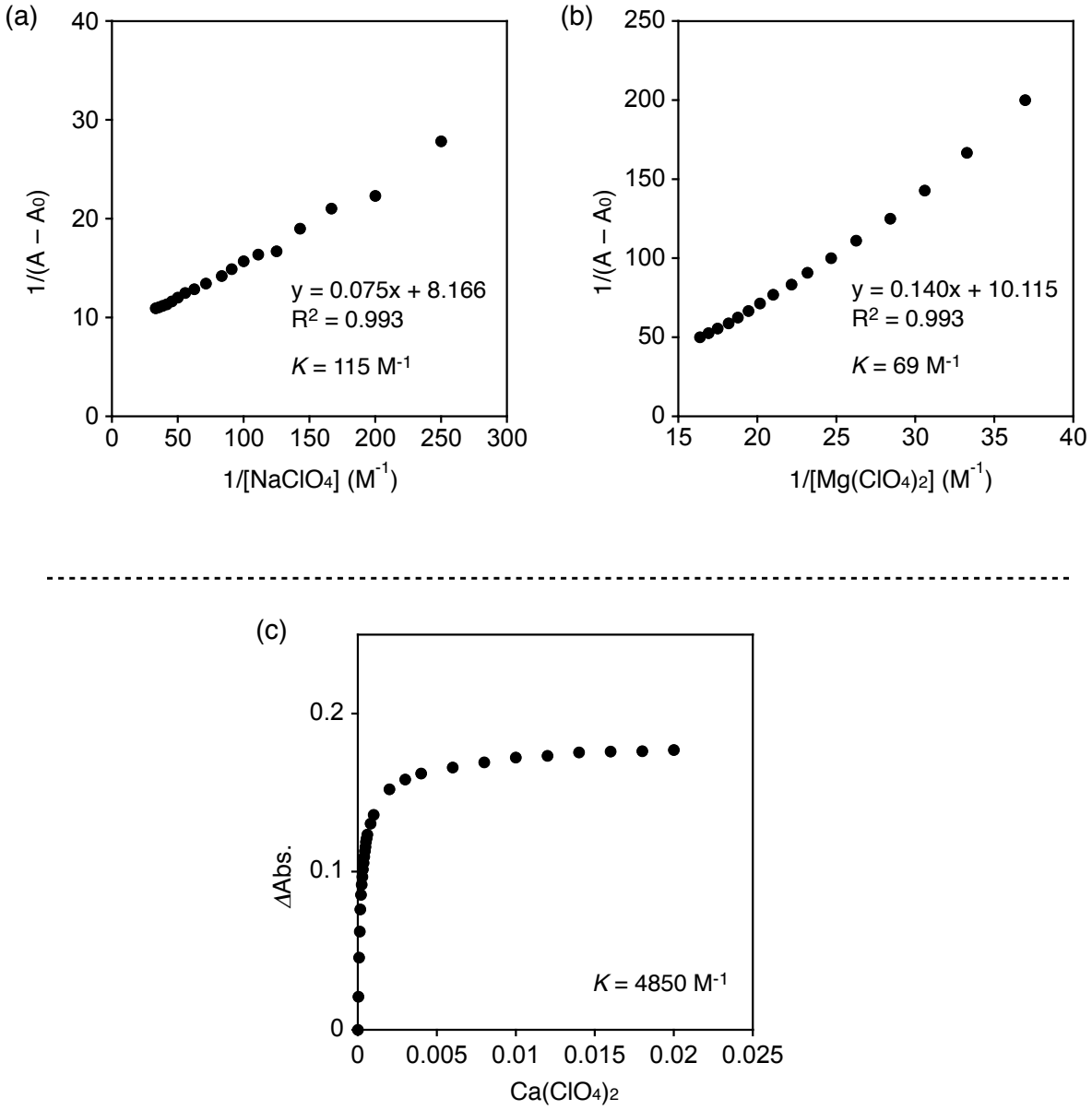

Figure S1. Benesi-Hildebrand plots of absorption spectral changes of $\mathbf{QE_3}$ upon titration with (a) $NaClO_4$ or (b) $Mg(ClO_4)_2$ in MeCN at 20 °C. (c) Plot of absorption spectral changes of $\mathbf{QE_3}$ upon titration with $Ca(ClO_4)_2$ in MeCN at 20 °C. The spectral change was monitored at λ_{max} of $\mathbf{QE_3}$ at 270 nm. [$\mathbf{QE_3}$] = 0.2 mM

2. ^{1}H NMR spectroscopy for a mixture of TME and $Pd(OAc)_2$

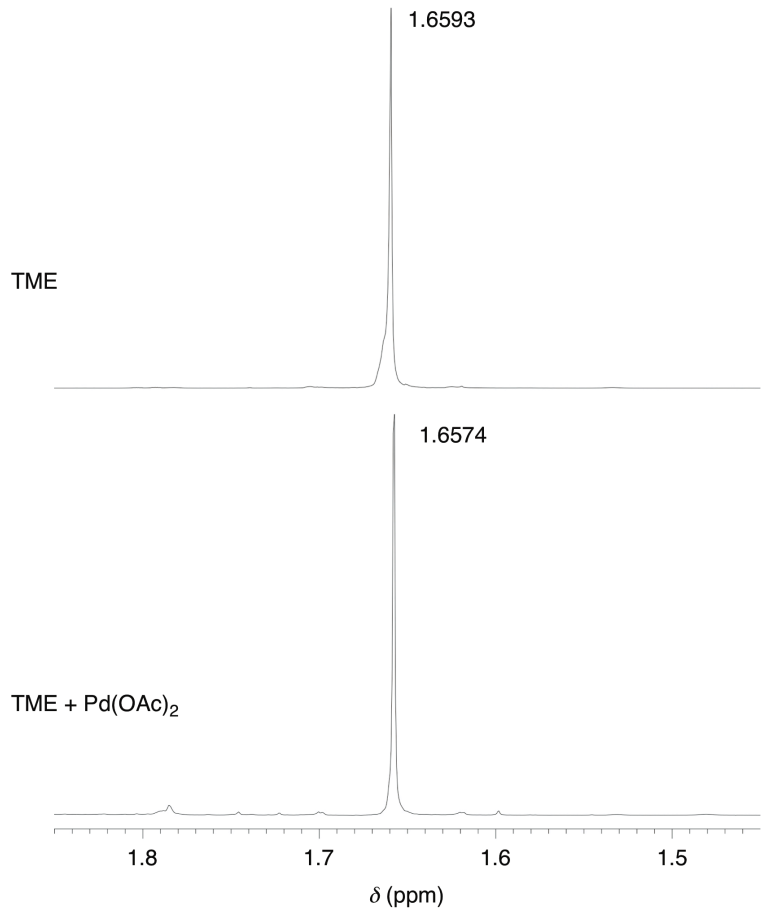

Figure S2. ^{1}H NMR spectrum of TME (top) and a 1:3 mixture of TME and $Pd(OAc)_2$ (bottom) in CD_3CN at 20 °C. [TME] = 10 mM, [$Pd(OAc)_2$] = 30 mM.

3. ^{1}H NMR spectroscopy for a ternary mixture of QE_3, TME, and $Pd(OAc)_2$

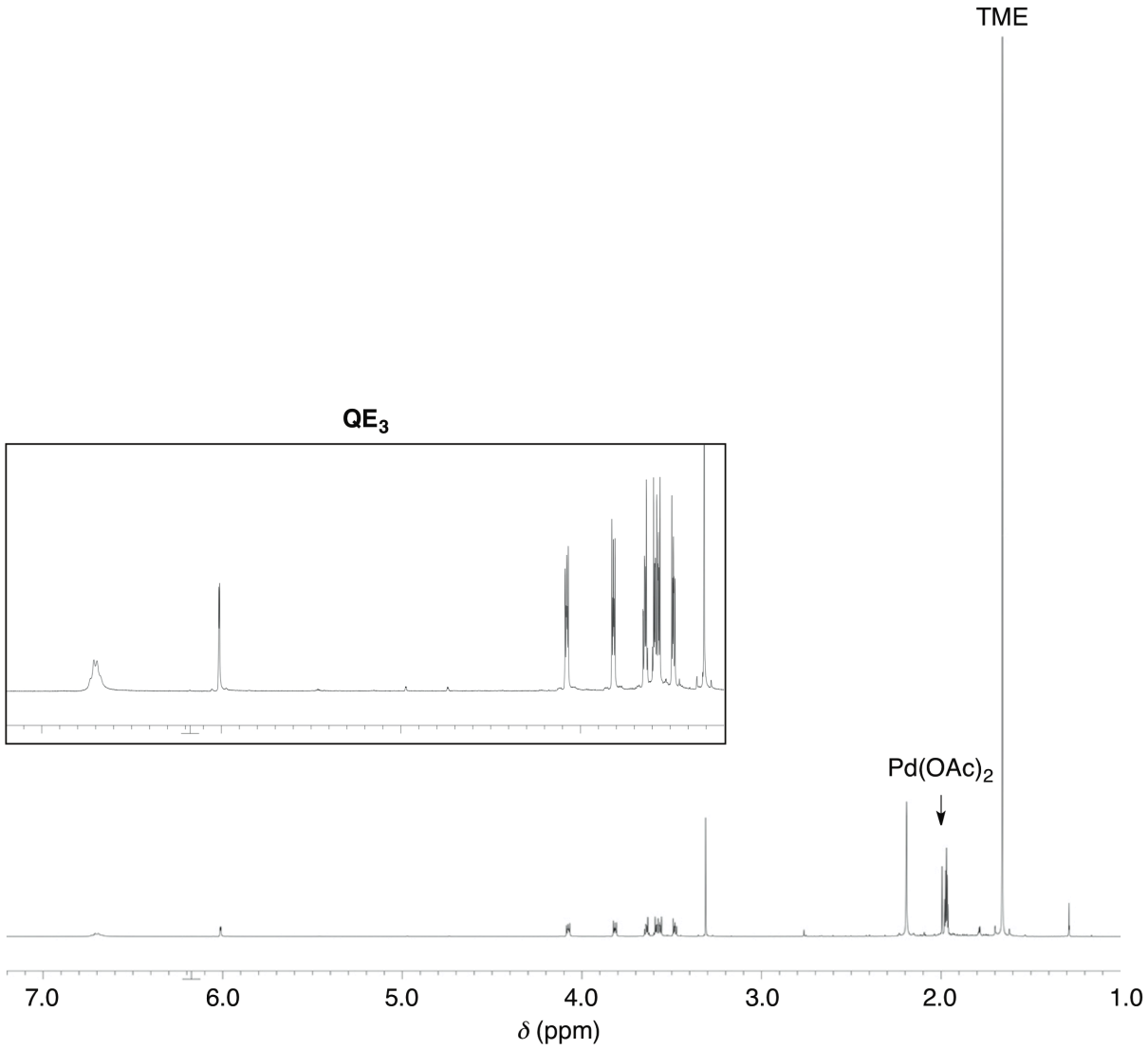

Figure S3. ^{1}H NMR spectrum of a 1:1:1 mixture of $\mathbf{QE_3}$, TME, and $Pd(OAc)_2$ in CD_3CN at 20 °C. [$\mathbf{QE_3}$] = [TME] = [$Pd(OAc)_2$] = 10 mM.

4. Cyclic voltammetry for mixtures of QE_3 and metal salt

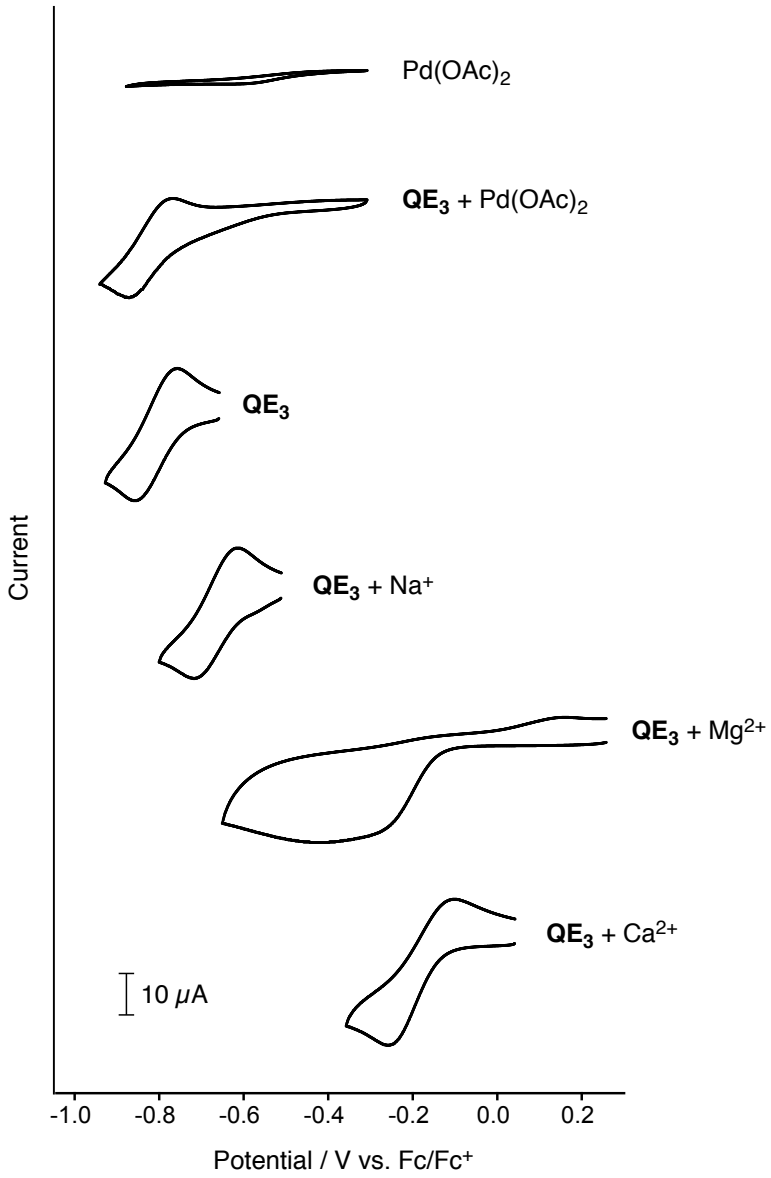

Figure S4. Redox profiles in cyclic voltammetry (V vs Fc/Fc^+) of $\mathbf{QE_3}$, $Pd(OAc)_2$, and mixtures of $\mathbf{QE_3}/NaClO_4$, $\mathbf{QE_3}/Mg(ClO_4)_2$, $\mathbf{QE_3}/Ca(ClO_4)_2$, and $\mathbf{QE_3}/Pd(OAc)_2$ in MeCN. Scan rate, 100 mV s^{-1}; working electrode, Pt; supporting electrolyte, 0.1 M Bu_4NClO_4. [$\mathbf{QE_3}$] = [$Pd(OAc)_2$] = 1.0 mM, [$NaClO_4$] = [$Mg(ClO_4)_2$] = [$Ca(ClO_4)_2$] = 10 mM

5. HPLC traces for the photochemical reactions of QE_n

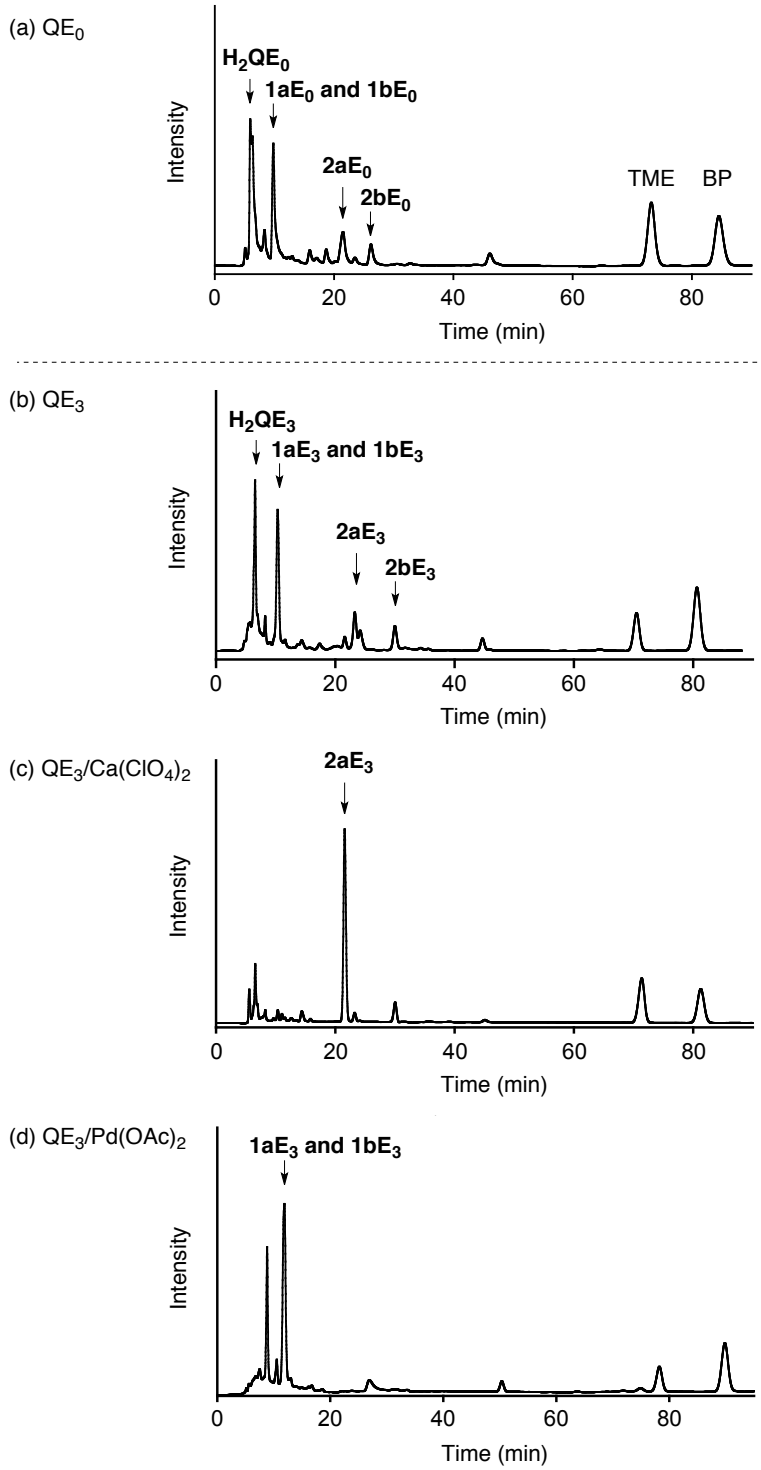

Figure S5. HPLC traces monitored at 220 nm for the product mixtures of the photochemical reactions of (a) $\mathbf{QE}_0$, (b) $\mathbf{QE}_3$, (c) $\mathbf{QE}_3/Ca(ClO_4)_2$, and (d) $\mathbf{QE}_3/Pd(OAc)_2$ with TME. BP: biphenyl as an internal standard.

6. X-ray crystallography of $2aE_0$

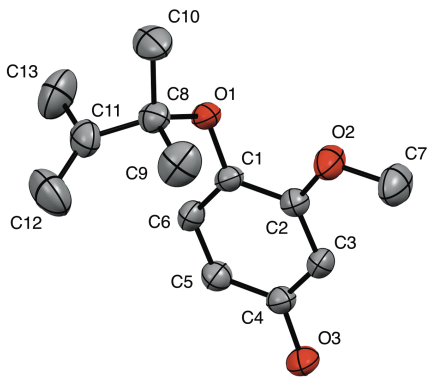

Figure S6. ORTEP diagram of **$2aE_0$**, using 50% probability ellipsoids. Hydrogen atoms are omitted for clarity (see ref. 3 and 4). X-ray diffraction data were collected on a Bruker SMART APEX II Ultra CCD diffractometer using Mo$K\alpha$ radiation (λ = 0.71073 Å) at 298 K. An empirical absorption correction was applied using the SADABS program. The structure was solved by the direct method and refined by full-matrix least-squares calculations on $F2$ using the SHELXTL 97 program package. All non-hydrogen atoms were refined anisotropically, and hydrogen atoms were added to calculated positions. The packing diagrams were drawn using ORTEP-3.

Crystal data and structure refinement

Empirical formula	$C_{13}H_{18}O_3$
Formula weight	222.27
Space group	monoclinic, P2(1)/c
Temperature	296 K
Wavelength	0.71073 Å
Crystal system	a = 7.0639 (16)
	b = 12.459 (3)
	c = 14.360 (3)
Unit cell volume	α = 90°
	β = 99.692°

	$\gamma = 90°$
Unit cell volume	1245.8 (5) $Å^3$
Z	4
F(000)	480.0
Crystal size	0.40 × 0.30 × 0.10 mm
Absorption coefficient	0.083 mm^{-1}
Data completeness	0.988
Theta (max)	27.440
Radiation	MoK¥a
Goodness of fit on F^2	1.227
R_{int}	0.0287
Final R indices [I>2sigma(I)]	$R_1 = 0.0455$, $wR_2 = 0.1584$
R indices (all date)	$R_1 = 0.0564$, $wR_2 = 0.1720$

7. Photodecomposition of QE_0

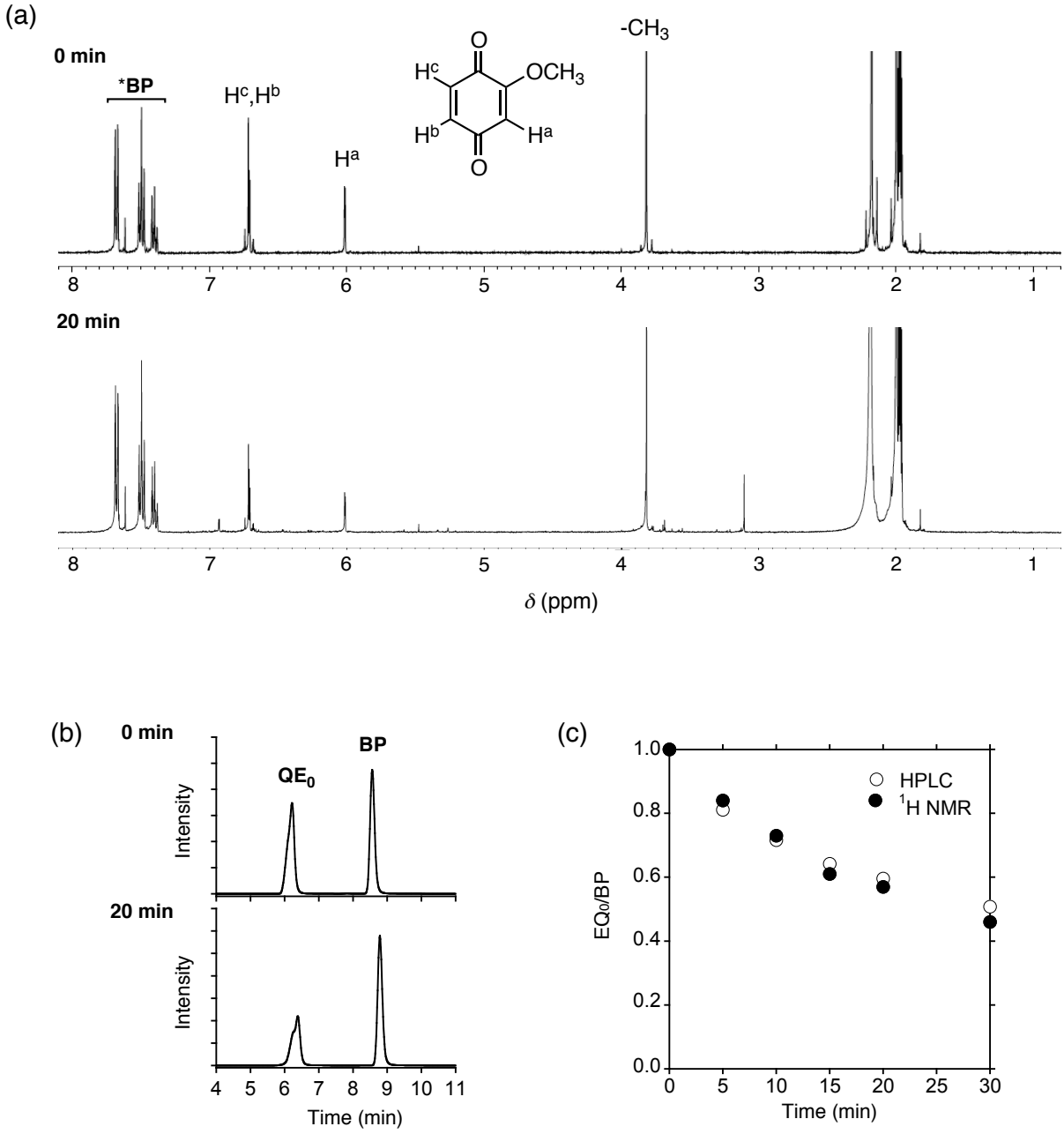

Figure S7. Decomposition of $\mathbf{QE_0}$ in CD_3CN at 20 °C upon photo-irradiation by 500 W xenon lamp equipped with a >420 nm optical filter, monitored by (a) ^{1}H NMR spectroscopy and (b) HPLC analysis. The amount of $\mathbf{QE_0}$ was evaluated from the peak integral ratio to biphenyl (**BP**) as an internal standard. (c) Plots of the ratio of $\mathbf{QE_0}$ to **BP**. [$\mathbf{QE_0}$] = 10 mM

8. Cyclic voltammetry of TME

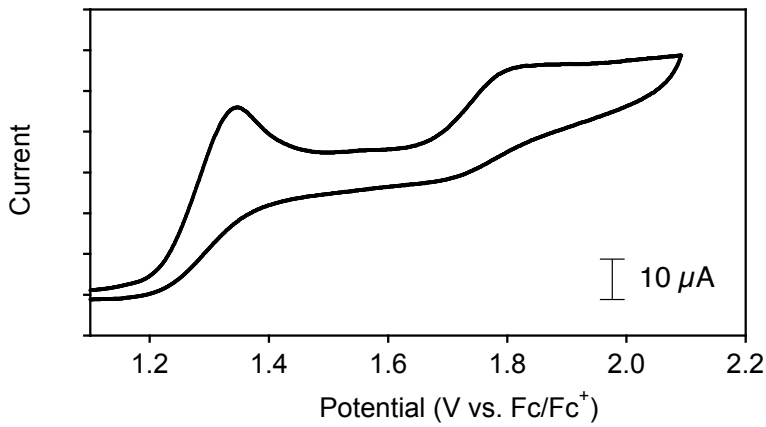

Figure S8. A redox profile in cyclic voltammetry (V vs Fc/Fc^+) of tetramethylethylene in MeCN. Scan rate, 100 mV s^{-1}; working electrode, Pt; supporting electrolyte, 0.1 M Bu_4NClO_4. [TME] = 1.0 mM

9. Phosphorescence spectra of QE_n in the absence or presence of metal salt

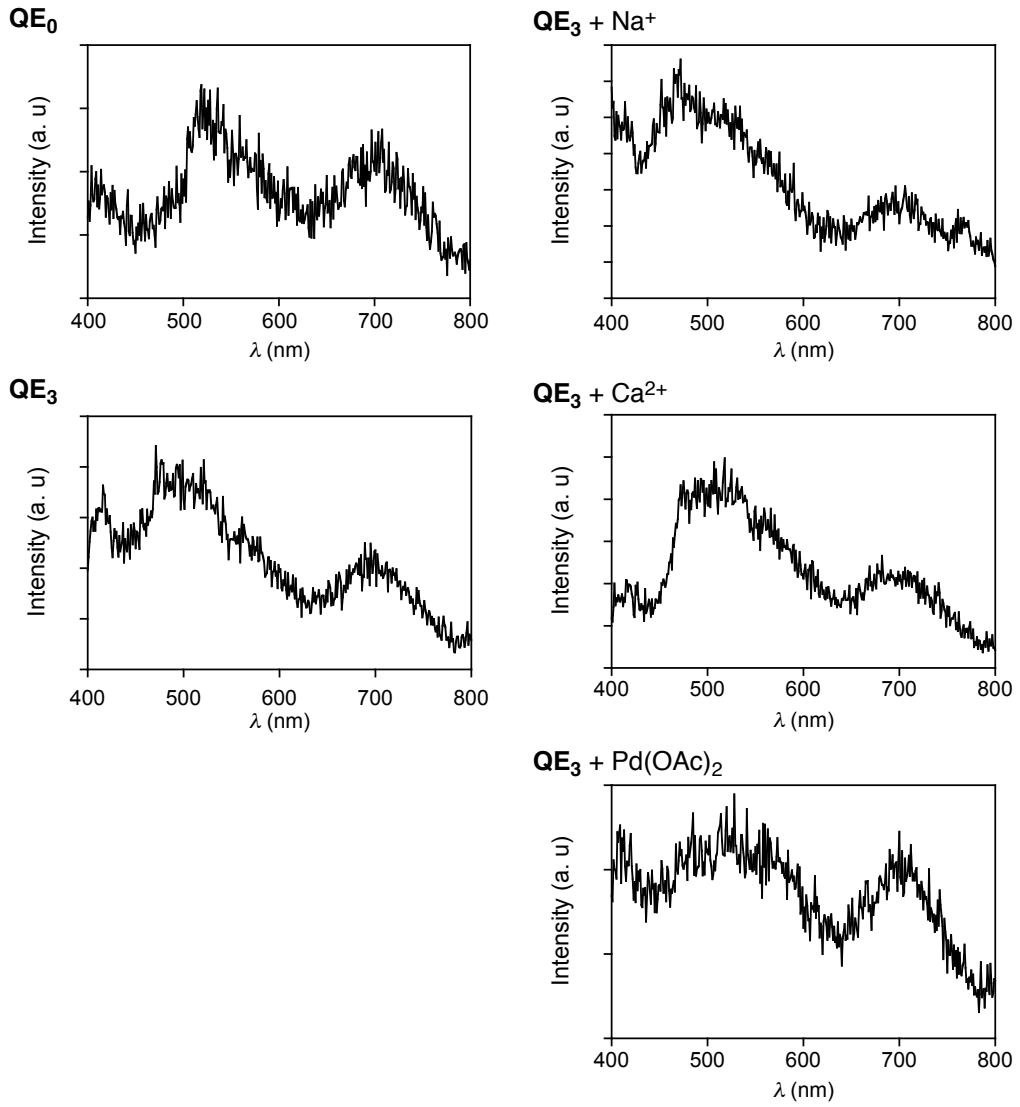

Figure S9. Phosphorescence spectra of $\mathbf{QE_0}$ and $\mathbf{QE_3}$ in the absence or presence of metal salt in MeCN glass at 77 K. Emission monochromator resolution and excitation band pass with excitation at 280 nm: 5.0 and 20.0 nm, respectively (see ref. 1).

10. Charge and spin densities of $QE_3^{\bullet-}$ and $QE_3^{\bullet-}\supset Ca(ClO_4)_2$ in DFT calculations with UB3LYP/6-31+G(d,p)

(see ref. 2)

$QE_3^{\bullet-}$

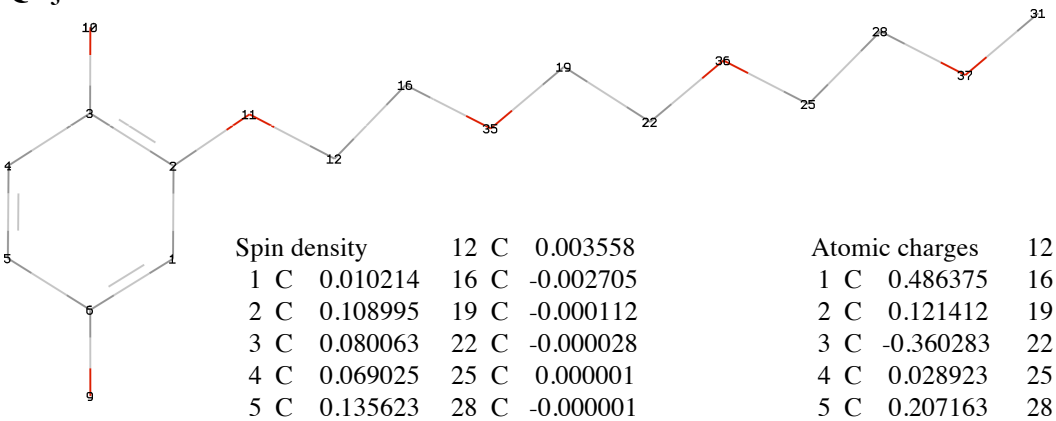

Spin density						Atomic charges					
1	C	0.010214	12	C	0.003558	1	C	0.486375	12	C	0.336778
2	C	0.108995	16	C	-0.002705	2	C	0.121412	16	C	-0.420760
3	C	0.080063	19	C	-0.000112	3	C	-0.360283	19	C	0.061179
4	C	0.069025	22	C	-0.000028	4	C	0.028923	22	C	-0.209638
5	C	0.135623	25	C	0.000001	5	C	0.207163	25	C	-0.034886
6	C	0.116224	28	C	-0.000001	6	C	-0.360630	28	C	-0.165184
9	O	0.218621	31	C	0.000000	9	O	-0.726048	31	C	-0.177198
10	O	0.257428	35	O	0.000094	10	O	-0.708401	35	O	-0.398376
11	O	0.014590	36	O	-0.000001	11	O	-0.400854	36	O	-0.401463
			37	O	0.000000				37	O	-0.389827

$QE_3^{\bullet-}\supset Ca(ClO_4)_2$

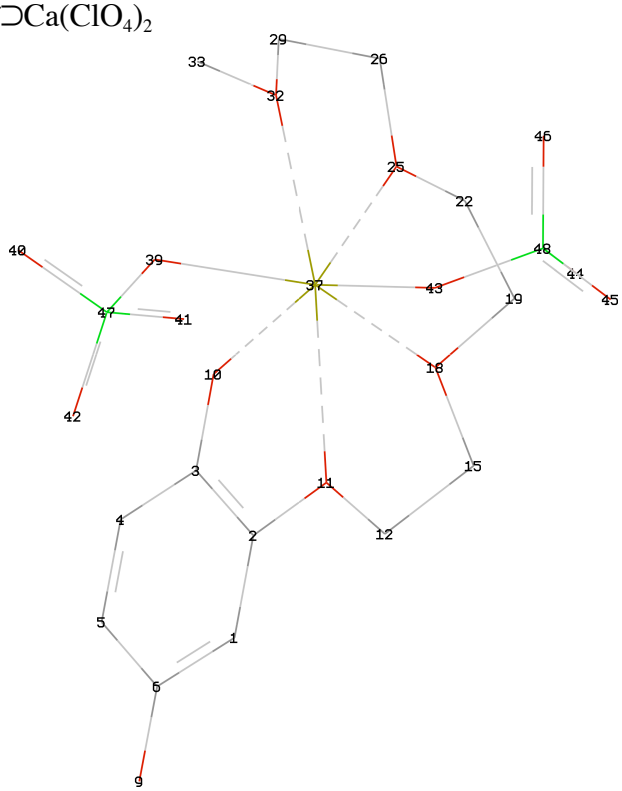

Spin density			Atomic charges		
1	C	0.071166	1	C	0.202566
2	C	0.063165	2	C	0.731048
3	C	0.158150	3	C	-0.055366
4	C	-0.017595	4	C	-0.888307
5	C	0.183216	5	C	0.153947
6	C	0.094733	6	C	-0.220909
9	O	0.246869	9	O	-0.679162
10	O	0.206159	10	O	-0.526343
11	O	0.006853	11	O	-0.371563
12	C	-0.002545	12	C	0.262017
15	C	0.001177	15	C	-0.255466
18	O	-0.000027	18	O	-0.399389
19	C	0.000051	19	C	0.100305
22	C	0.000112	22	C	-0.231050
25	O	0.000117	25	O	-0.389221
26	C	0.000061	26	C	-0.152000
29	C	-0.000167	29	C	-0.064454
32	O	0.000030	32	O	-0.385323
33	C	0.000077	33	C	-0.141869
37	Ca	0.000197	37	Ca	1.228496
39	O	0.000508	39	O	-0.642469
40	O	0.000085	40	O	-0.523286
41	O	0.000132	41	O	-0.510003
42	O	0.000421	42	O	-0.498303
43	O	0.001260	43	O	-0.634325
44	O	0.000084	44	O	-0.517821
45	O	0.000144	45	O	-0.504070
46	O	0.000175	46	O	-0.503131
47	Cl	-0.000036	47	Cl	1.290809
48	Cl	-0.001049	48	Cl	1.268391

11. Charge and spin densities of $QE_0^{\bullet-}$ and $QE_0^{\bullet-}/Pd(OAc)_2$ in DFT calculations with UB3PW91/LANL2DZ

$QE_0^{\bullet-}$

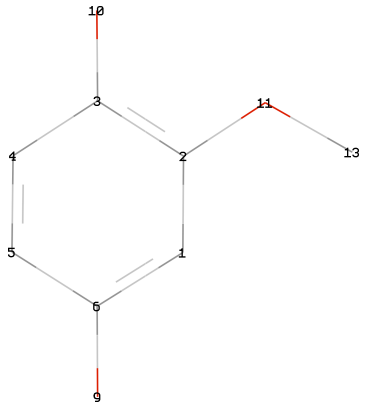

Spin density			Atomic charges		
1	C	-0.487438	1	C	-0.487438
2	C	0.267825	2	C	0.267825
3	C	0.047194	3	C	0.047194
4	C	-0.279242	4	C	-0.279242
5	C	-0.348669	5	C	-0.348669
6	C	0.039172	6	C	0.151874
9	O	0.286203	9	O	-0.420262
10	O	0.334053	10	O	-0.375564
11	O	0.014028	11	O	-0.302369
13	C	-0.001680	13	C	-0.504549

$QE_0^{\bullet-}/Pd(OAc)_2$

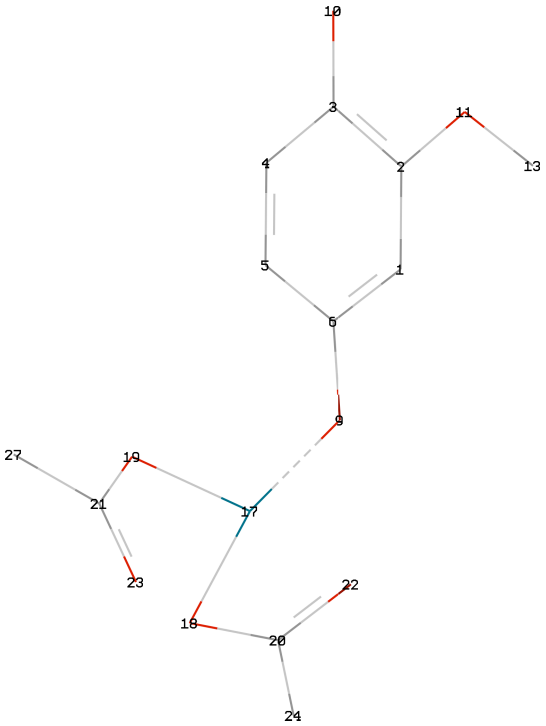

Spin density			Atomic charges		
1	C	-0.082228	1	C	-0.485149
2	C	0.165940	2	C	0.266031
3	C	-0.020573	3	C	0.062851
4	C	0.163932	4	C	-0.297456
5	C	-0.002765	5	C	-0.284537
6	C	0.206394	6	C	0.390323
9	O	0.158102	9	O	-0.444324
10	O	0.390051	10	O	-0.323317
11	O	0.029775	11	O	-0.290003
13	C	-0.003445	13	C	-0.505852
17	Pd	0.044351	17	Pd	0.425708
18	O	0.113524	18	O	-0.394485
19	O	-0.053260	19	O	-0.459225
20	C	-0.127328	20	C	0.460679
21	C	0.134163	21	C	0.427788
22	O	0.119734	22	O	-0.394819
23	O	-0.167580	23	O	-0.356857
24	C	0.966156	24	C	-0.526914
27	C	-1.035293	27	C	-0.519643

12. Formation of 2,3-dimethyl-1,3-butadiene in the photochemical reaction

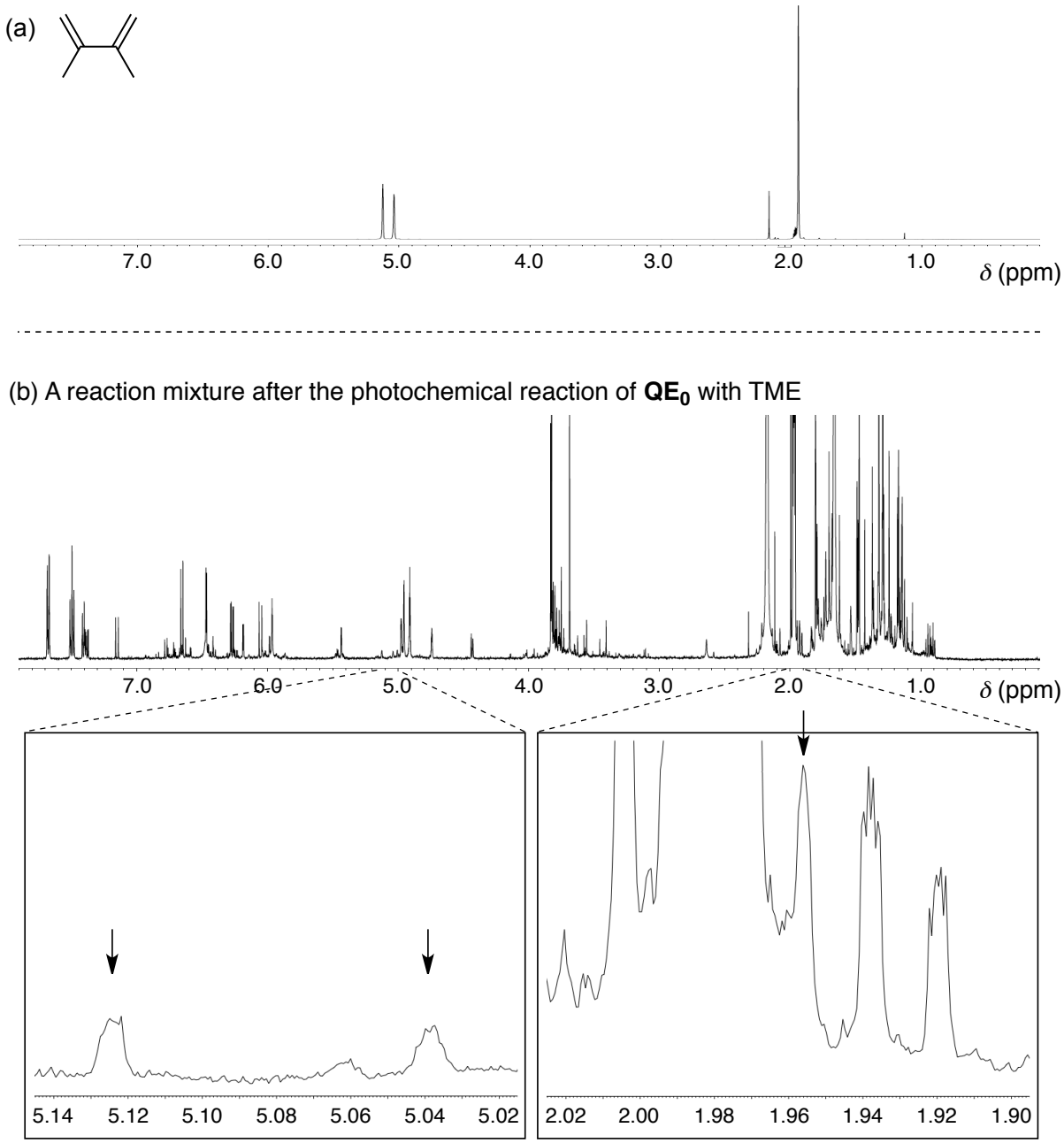

Figure S10. ^{1}H NMR spectroscopy of (a) 2,3-dimethyl-1,3-butadiene and (b) product mixtures obtained after photo-irradiation of $\mathbf{QE_0}$ with TME by 500 W xenon lamp equipped with a >420 nm optical filter at 20 °C. Solvent: CD_3CN, [$\mathbf{QE_0}$] = 10 mM, [TME] = 40 mM.

13. Photochemical reaction of QE_0 with TME in the presence of $Pd(OAc)_2$

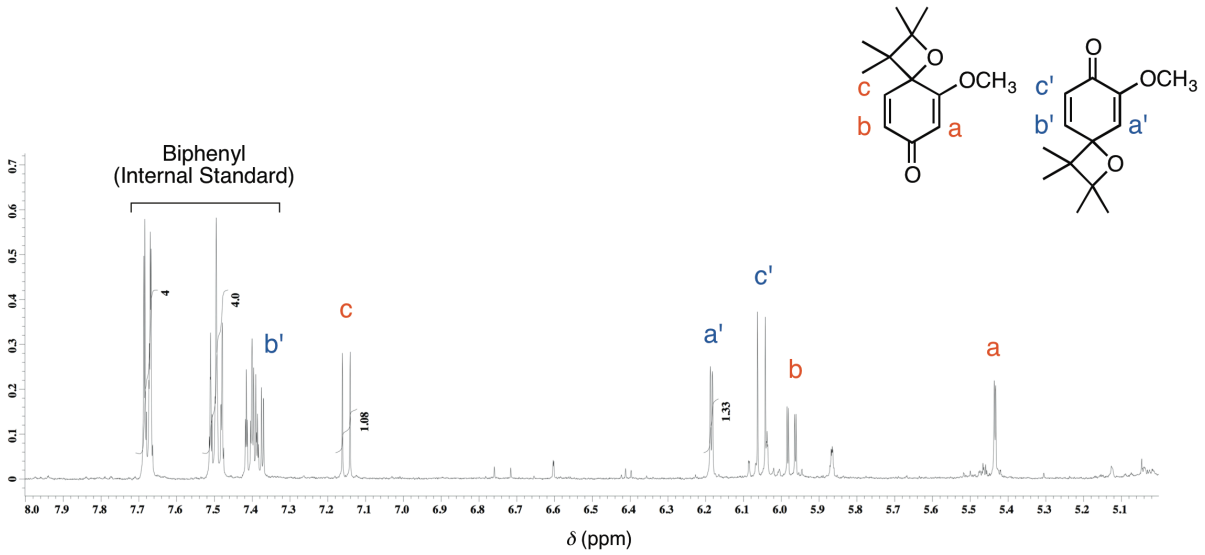

Figure S11. ^{1}H NMR spectrum of a reaction mixture obtained after photo-irradiation of $\mathbf{QE_0}$ with TME in the presence of $Pd(OAc)_2$ in CD_3CN at 20 °C. [$\mathbf{QE_0}$] = [$Pd(OAc)_2$] = 10 mM, [TME] = 40 mM

14. Photochemical reaction of QE_3 with TME in the presence of $Pd(OAc)_2$

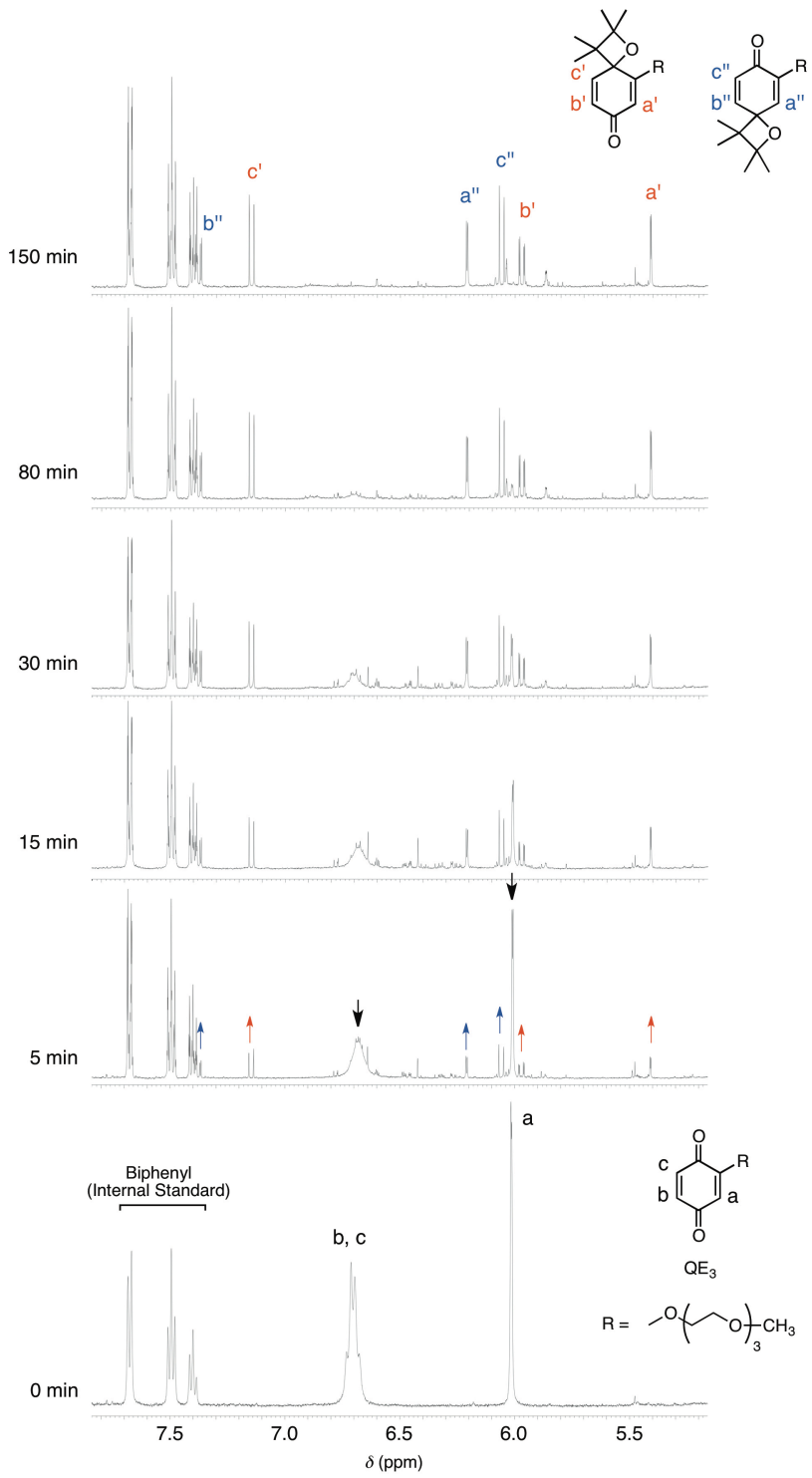

Figure S12. Changes in ^{1}H NMR spectra of a photochemical reaction of $\mathbf{QE_3}$ with TME in the presence of $Pd(OAc)_2$ in CD_3CN at 20 °C with respect to the reaction time. [$\mathbf{QE_3}$] = [$Pd(OAc)_2$] = 10 mM, [TME] = 40 mM

15. Photochemical reaction of QE_3 with TME in the presence of $Pd(OAc)_2$ (continued)

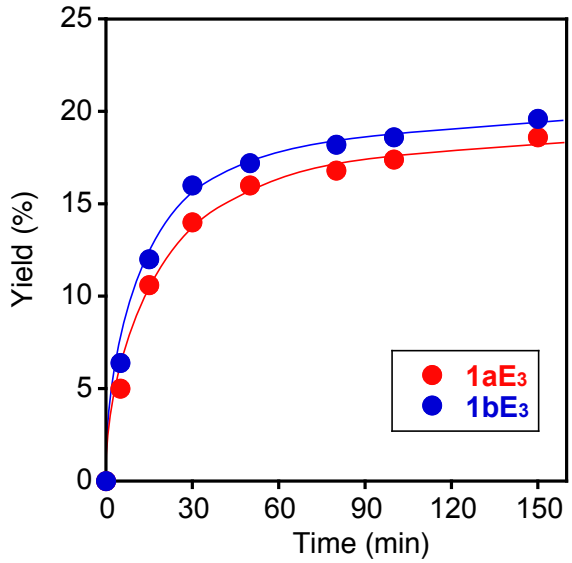

Figure S13. Plots of the yields of **1aE$_3$** and **1bE$_3$** in the product mixture of the photochemical reaction of **QE$_3$** with TME in the presence of $Pd(OAc)_2$ in CD_3CN at 20 °C. [**QE$_3$**] = [$Pd(OAc)_2$] = 10 mM, [TME] = 40 mM

16. Hyperfine coupling constants predicted by DFT calculations

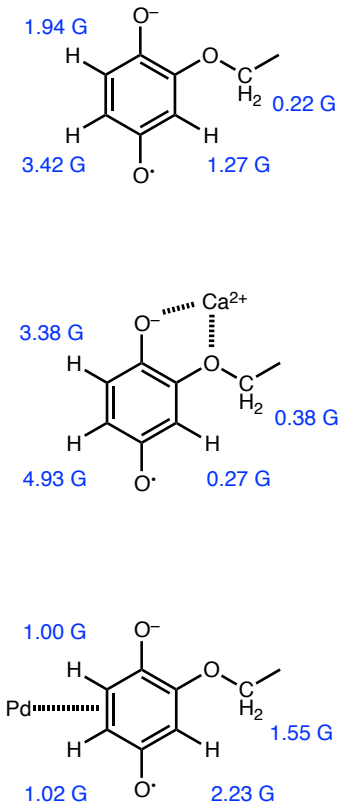

Figure S14. Calculated values of the hyperfine coupling constants of $\mathbf{QE_3}^{\bullet-}$, $\mathbf{QE_3}^{\bullet-}/Ca^{2+}$ complex, and $\mathbf{QE_3}^{\bullet-}/Pd(OAc)_2$ complex by DFT with UB3LYP/6-311G(d) or UB3LYP/LANL2DZ level.

17. Detection of a palladium-complex of QE_3 generated upon photo-irradiation in ESI-FT-MS

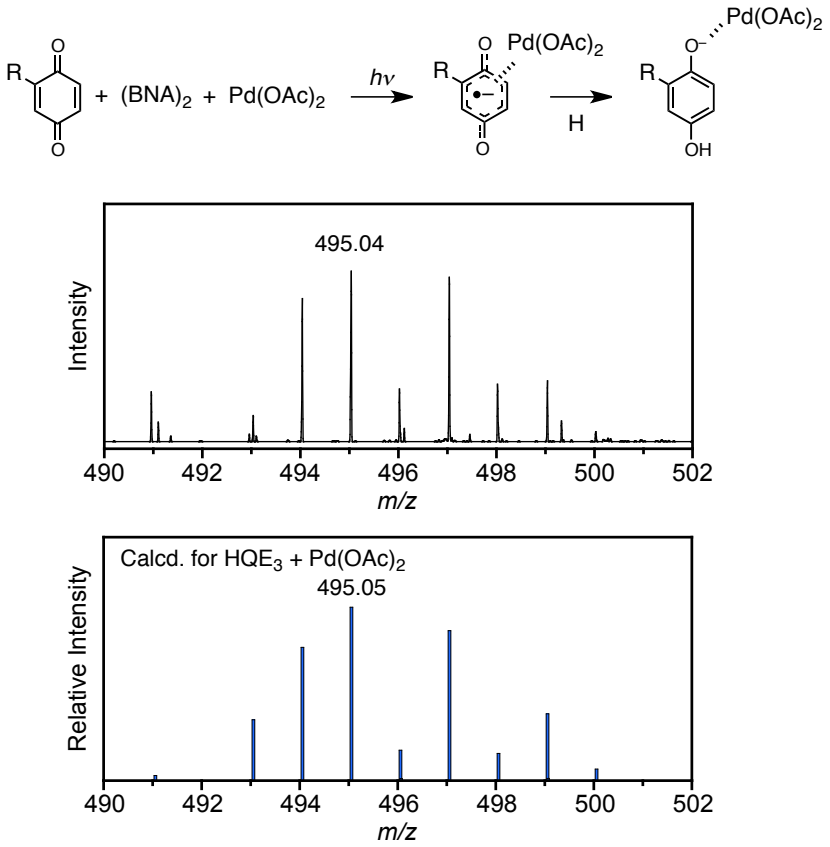

Figure S15. Observed peaks in the range of *m/z* = 490–502 in negative mode ESI-FT-MS of a photo-irradiated MeCN solution, containing a mixture of $\mathbf{QE_3}$, $(BNA)_2$, and $Pd(OAc)_2$ ([$\mathbf{QE_3}$] = [$(BNA)_2$] = [$Pd(OAc)_2$] = 3.0 mM) with the calculated isotope pattern of a mono hydrolyzed $\mathbf{QE_3}^{\bullet-}/Pd(OAc)_2$ complex. The measurement was performed on a Thermo Fisher Scientific LTQ Orbitrap Discovery. The sample solution was prepared upon photo-irradiation of a MeCN solution, containing a mixture of $\mathbf{QE_3}$, $(BNA)_2$, and $Pd(OAc)_2$ with the concentrations of 3.0 mM, respectively, with a 4 W white LED lamp for 10 sec. The sample was ionized by negative electrospray ionization with source voltage and capillary temperature of 1.5 kV and 200 °C, respectively.

18. Changes in ESR spectrum of $QE_3^{\bullet-}/TME^{\bullet+}$ upon metal binding

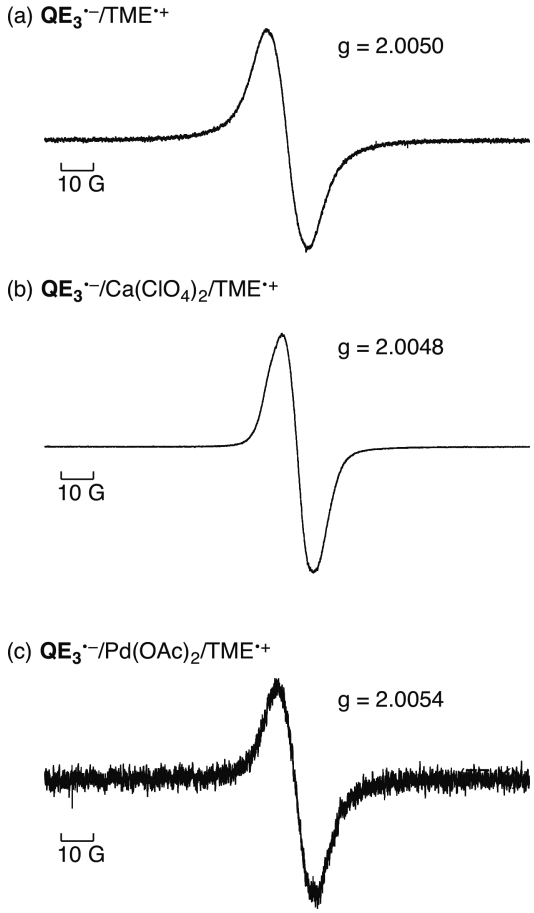

Figure S16. ESR spectra of (a) $\mathbf{QE_3}^{\bullet-}/TME^{\bullet+}$ complex, (b) $\mathbf{QE_3}^{\bullet-}/Ca(ClO_4)_2/TME^{\bullet+}$ complex, and (c) $\mathbf{QE_3}^{\bullet-}/Pd(OAc)_2/TME^{\bullet+}$ complex generated by the photo-irradiation of a mixture of $\mathbf{QE_3}$ (10.0 mM) and TME (40.0 mM) in the absence or presence of $Ca(ClO_4)_2$ (100.0 mM) or $Pd(OAc)_2$ (10.0 mM) in deaerated MeCN at 77 K.

19. ^{1}H and ^{13}C NMR spectra of products

(a) ^{1}H and ^{13}C NMR spectra of **1aE$_0$** in $CDCl_3$

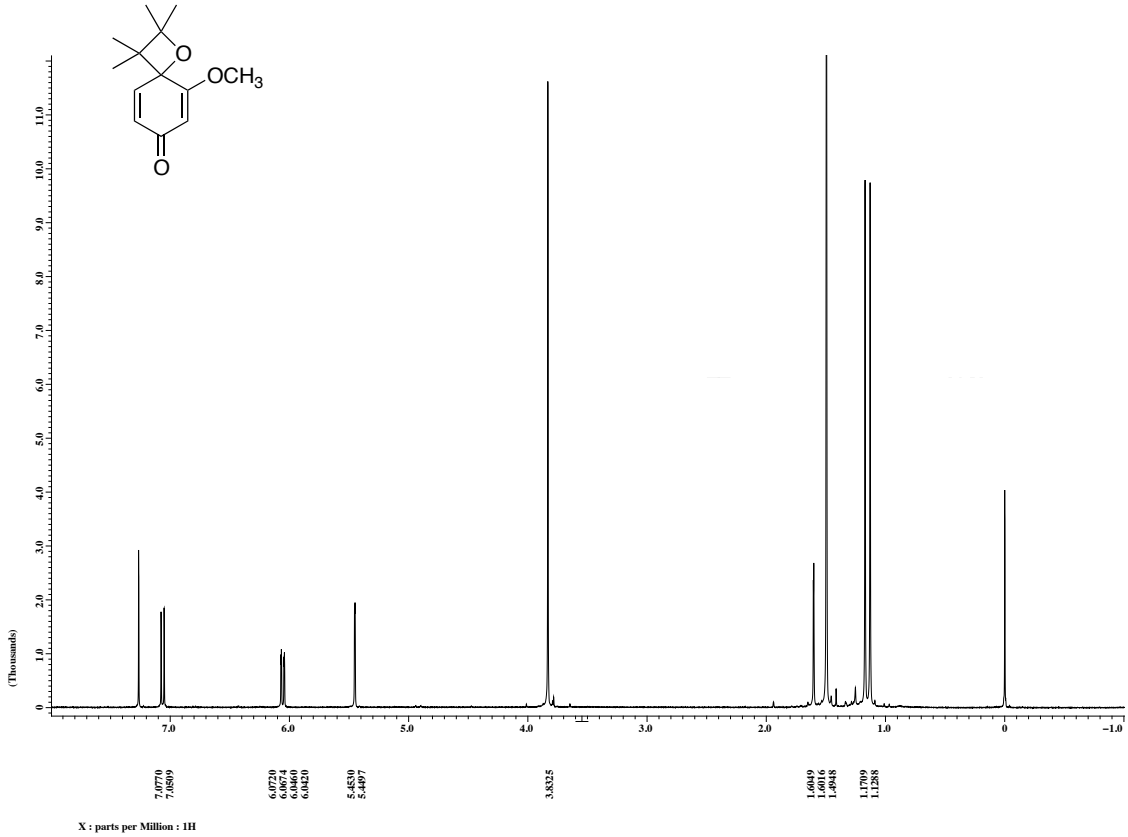

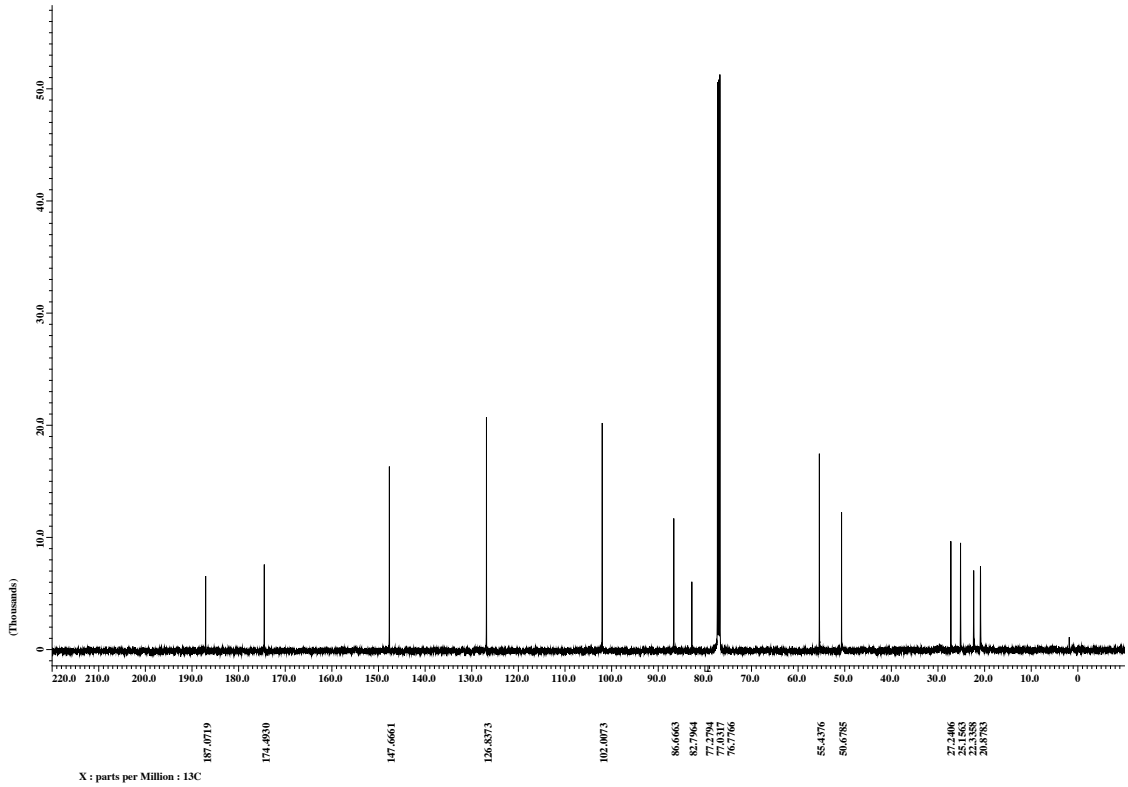

$^{1}H–^{1}H$ NOESY spectrum of **1aE$_0$**

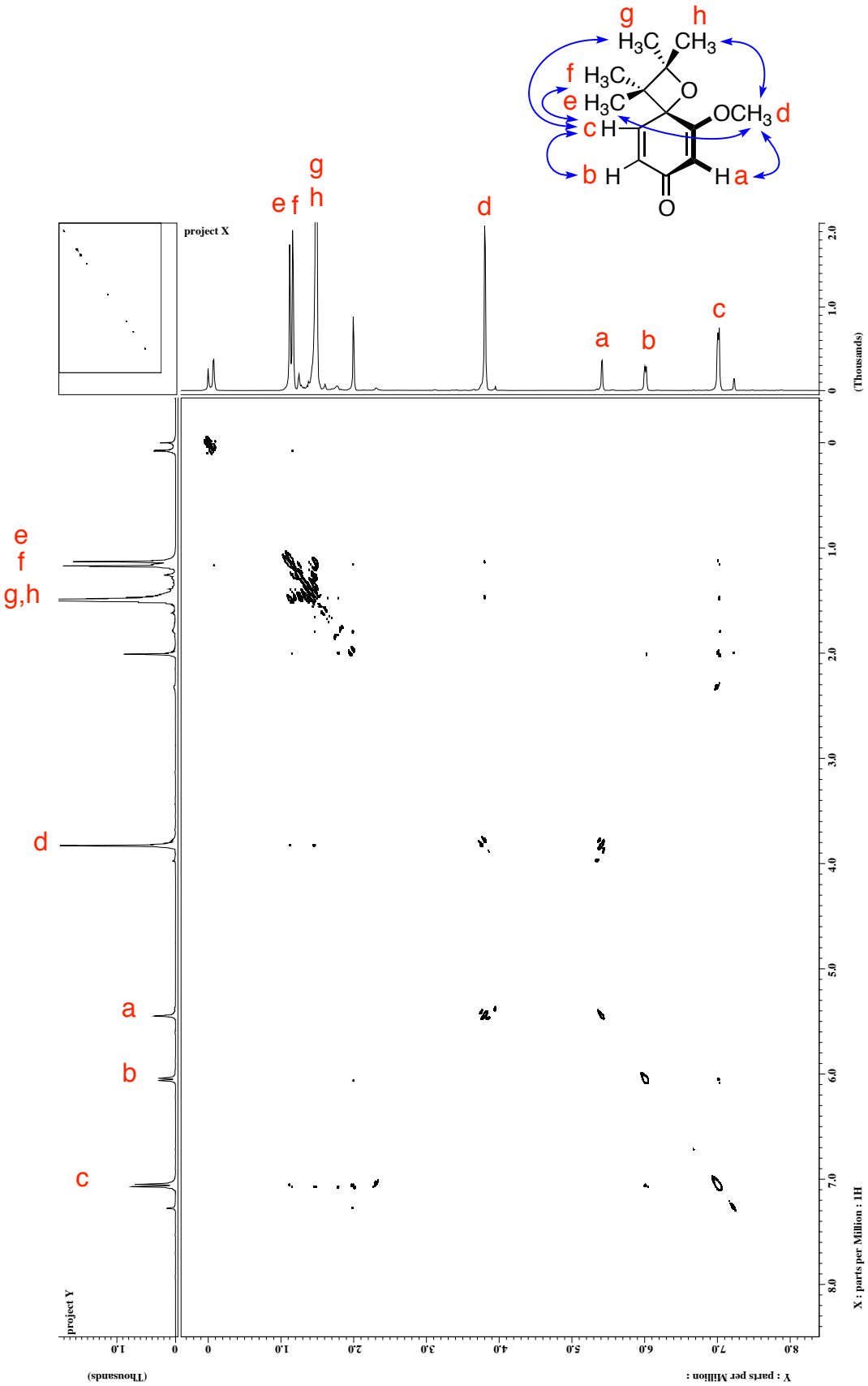

(b) ^{1}H and ^{13}C NMR spectra of **1bE$_0$** in $CDCl_3$

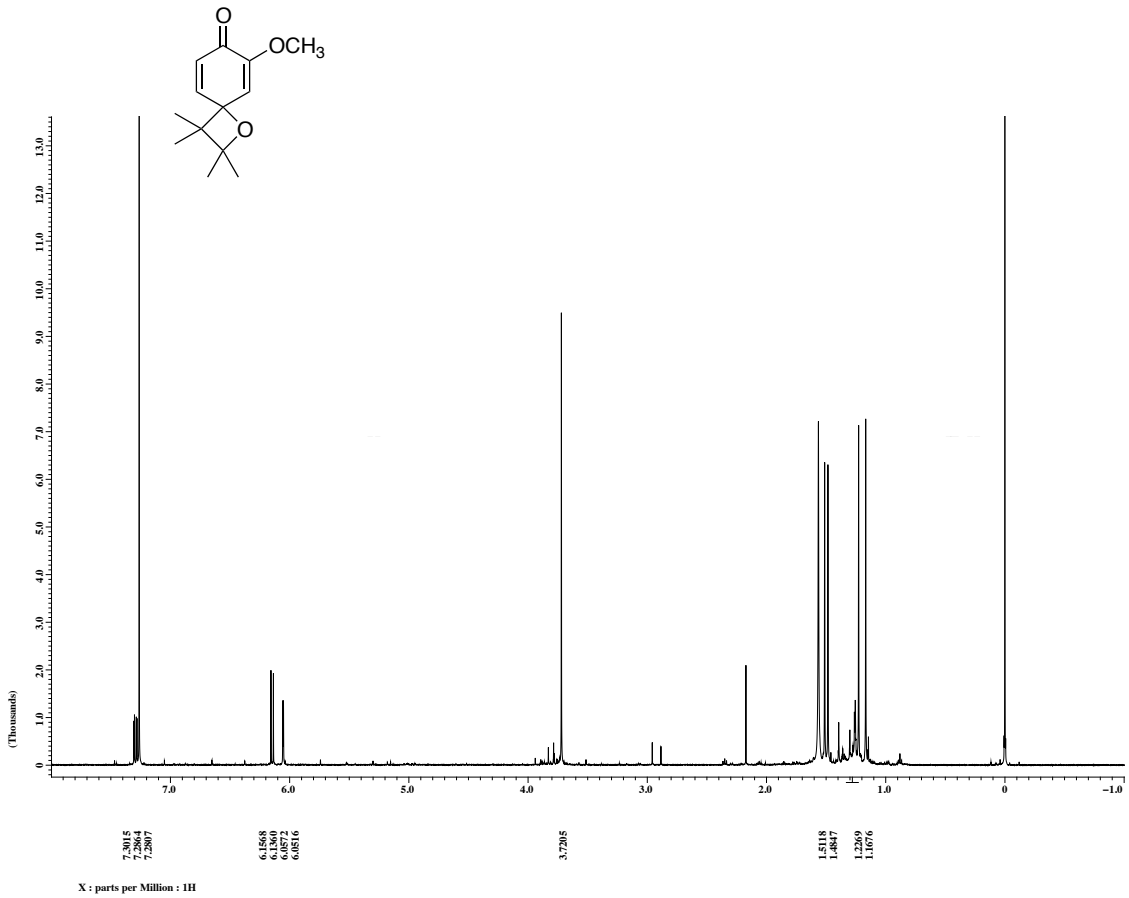

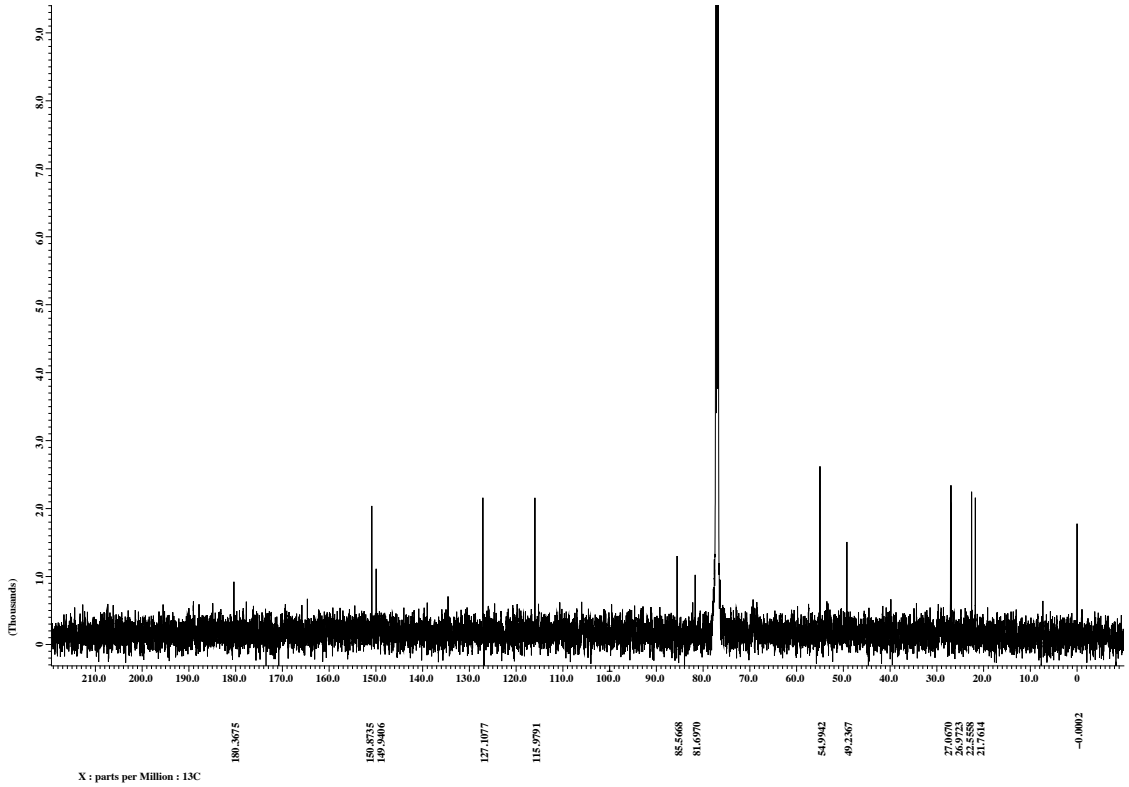

$^{1}H–^{1}H$ NOESY spectrum of **1bE$_0$**

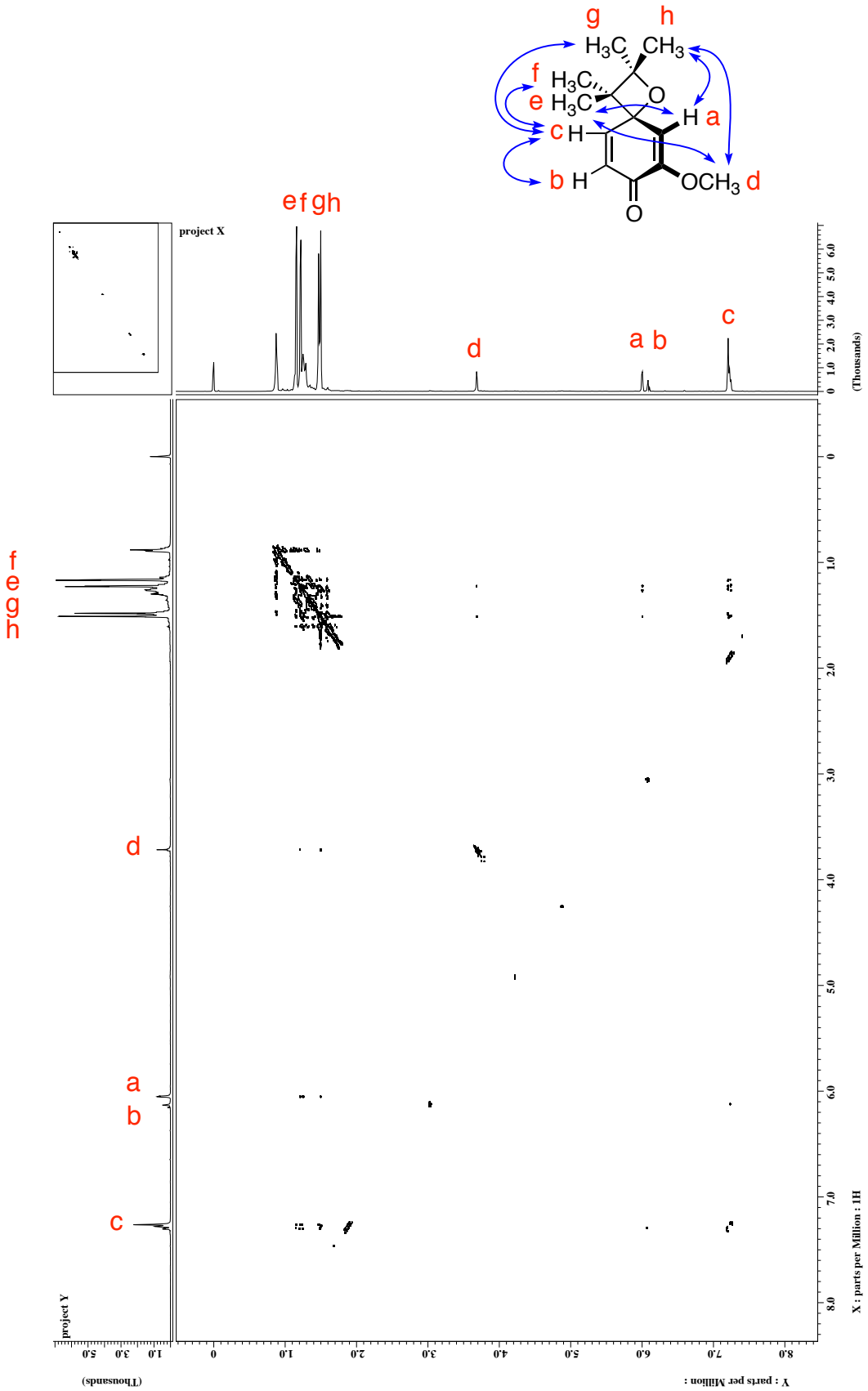

(c) ^{1}H and ^{13}C NMR spectra of **2aE$_0$** in $CDCl_3$

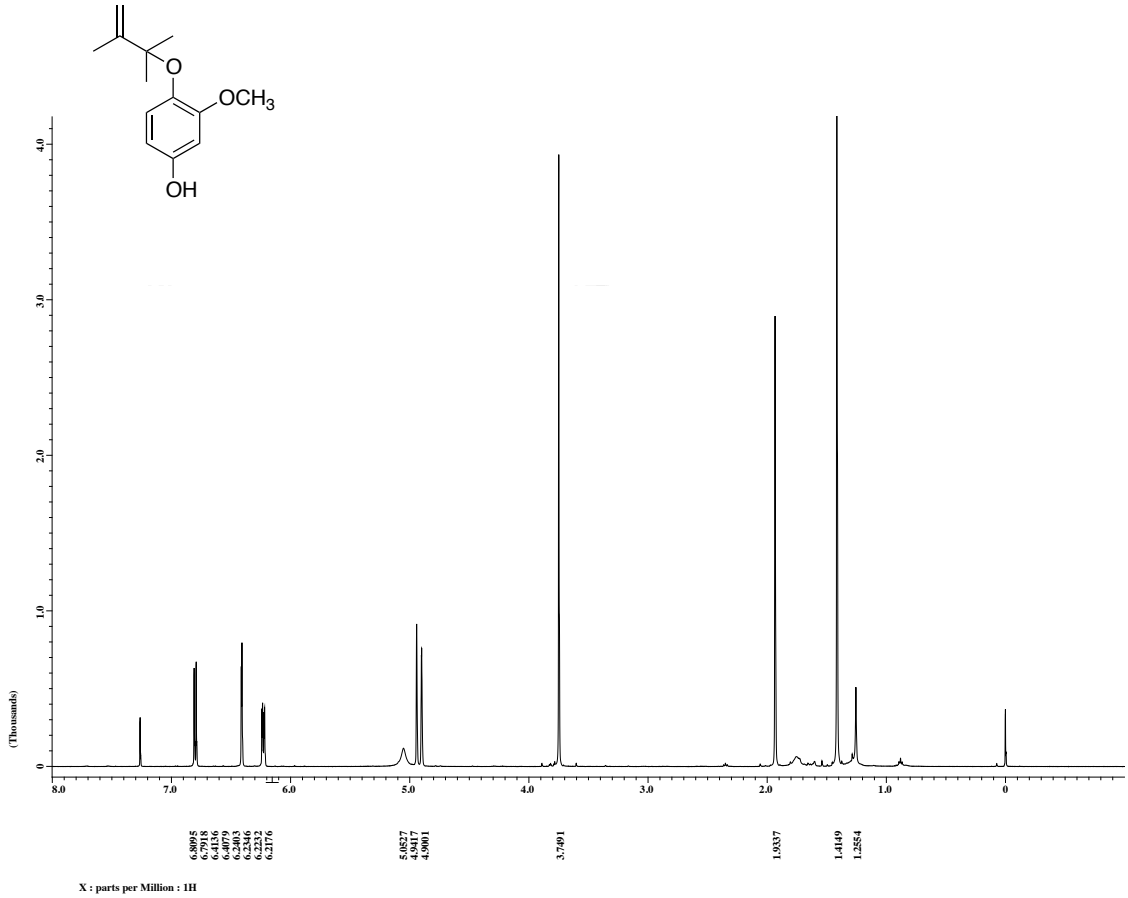

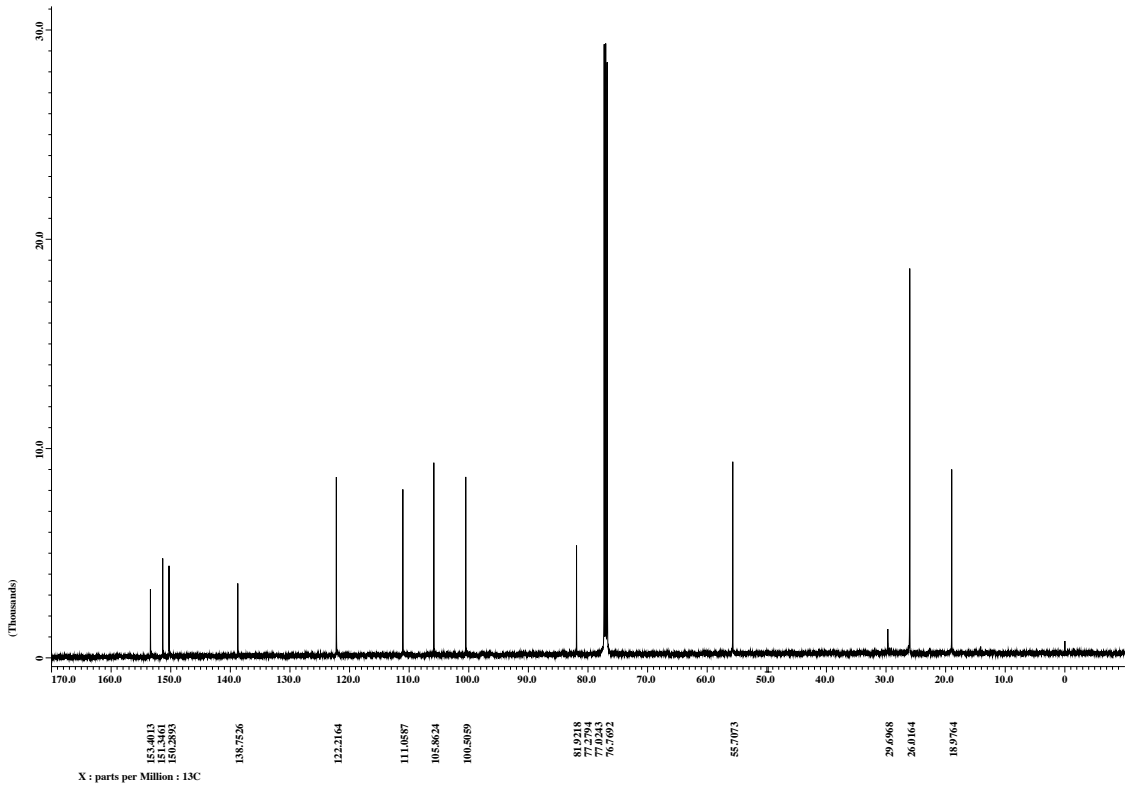

(d) ^{1}H and ^{13}C NMR spectra of **2bE$_0$** in $CDCl_3$

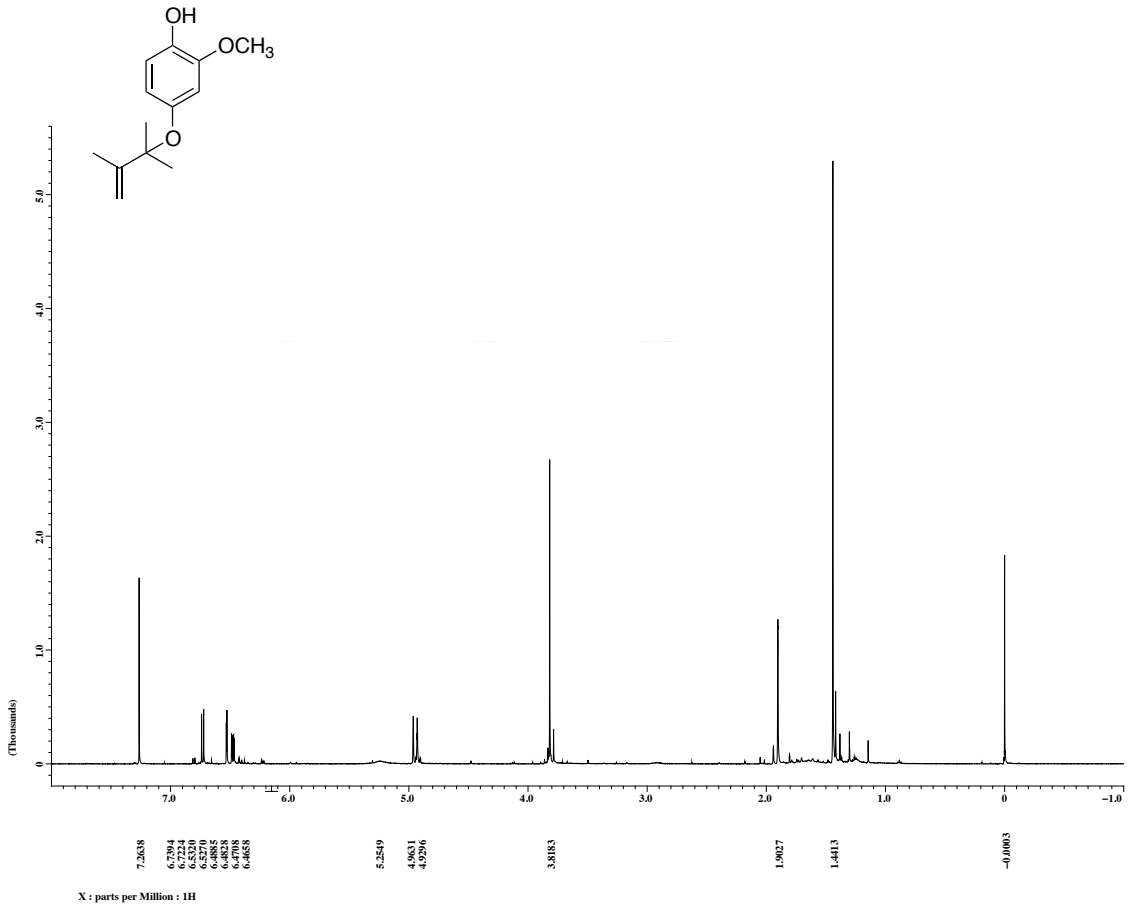

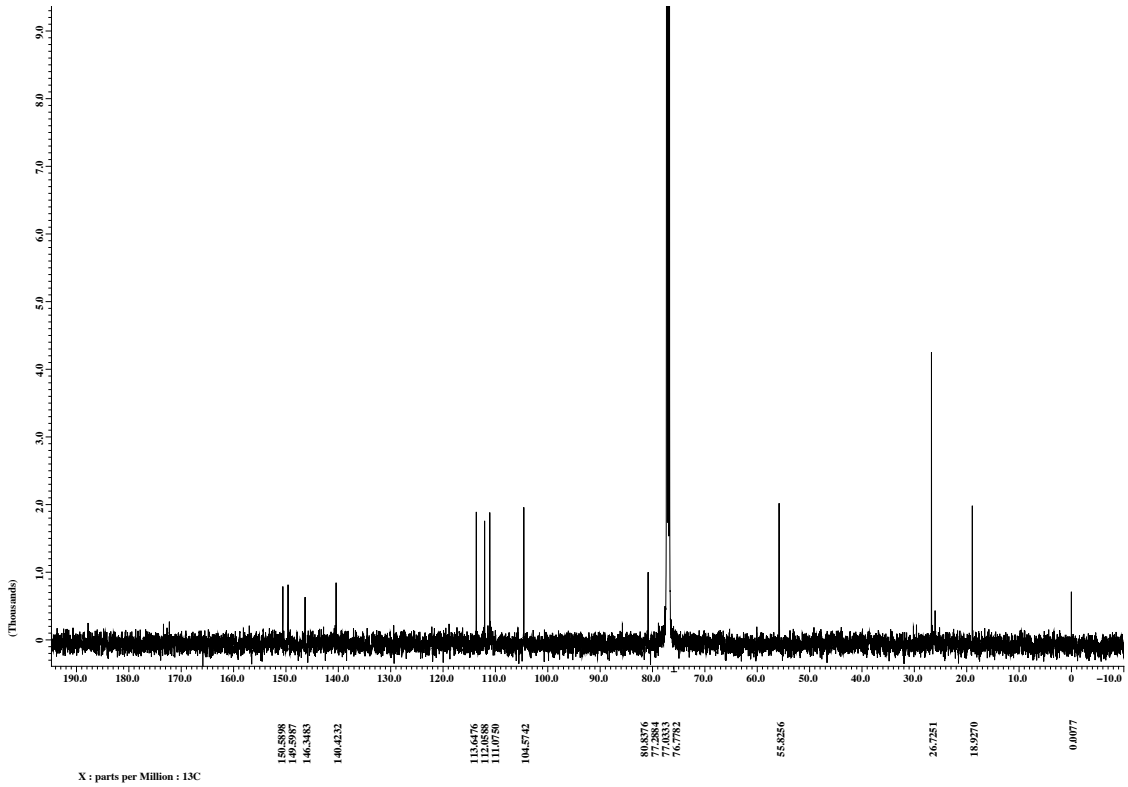

(e) ^{1}H and ^{13}C NMR spectra of **1aE$_3$** in $CDCl_3$

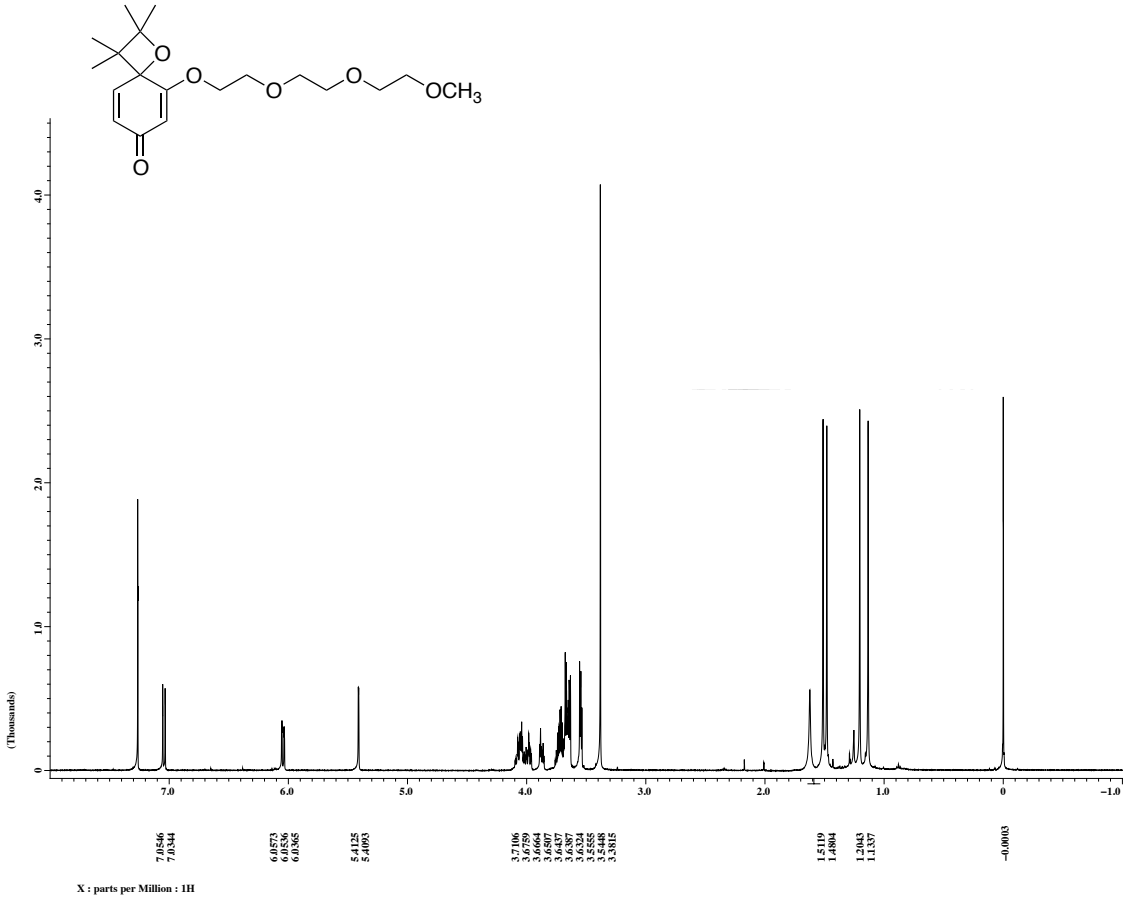

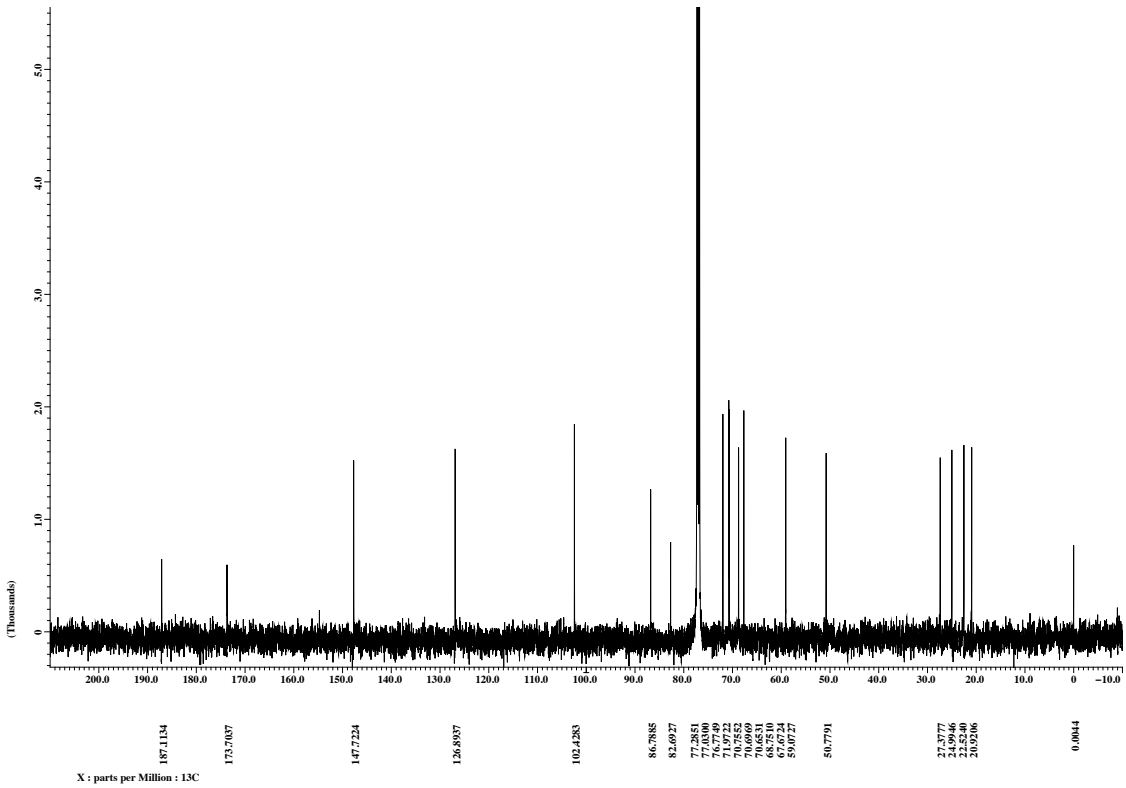

(f) ^{1}H and ^{13}C NMR spectra of **1bE$_3$** in $CDCl_3$

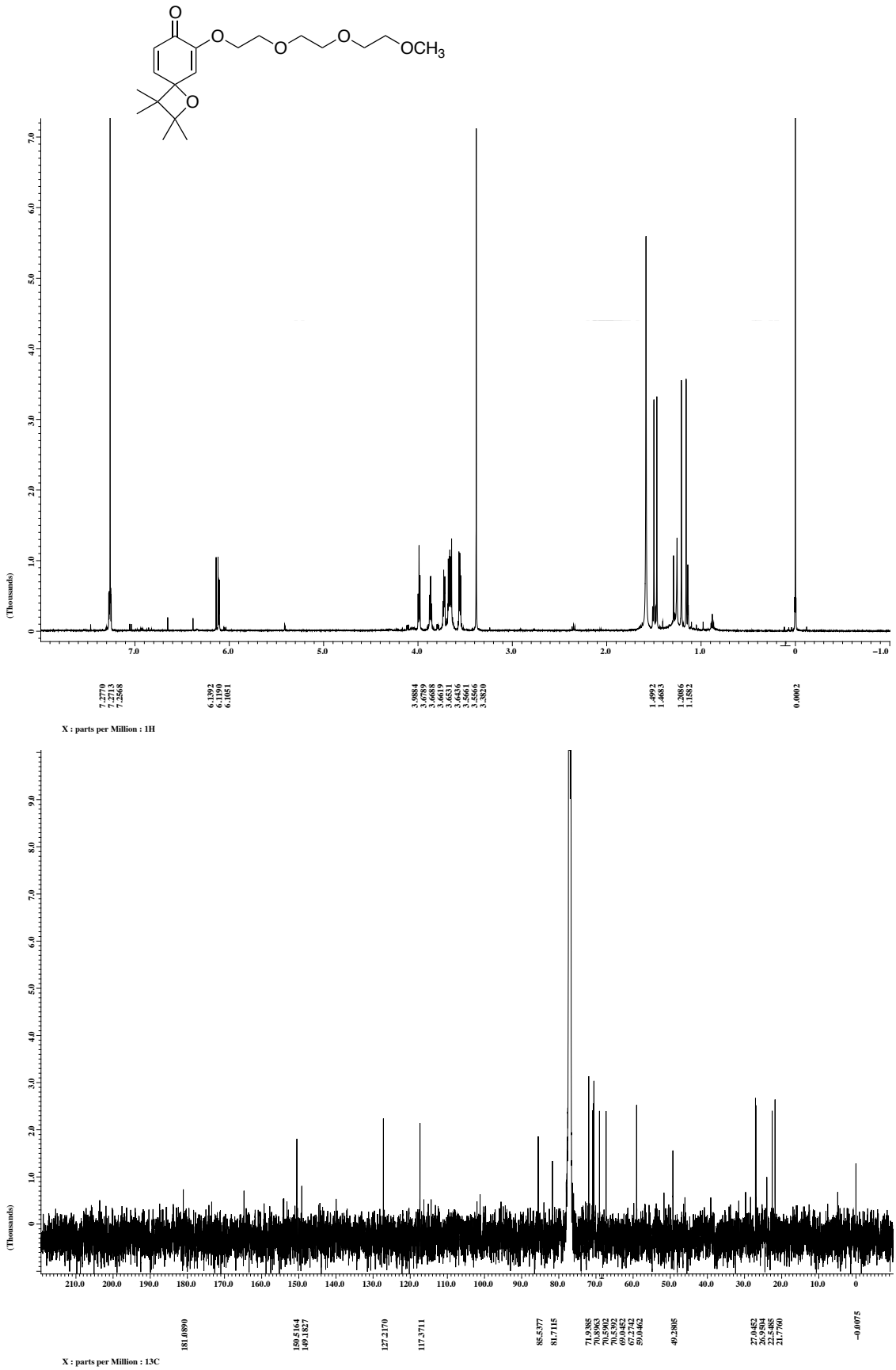

(g) ^{1}H and ^{13}C NMR spectra of **H_2QE_3** in $CDCl_3$

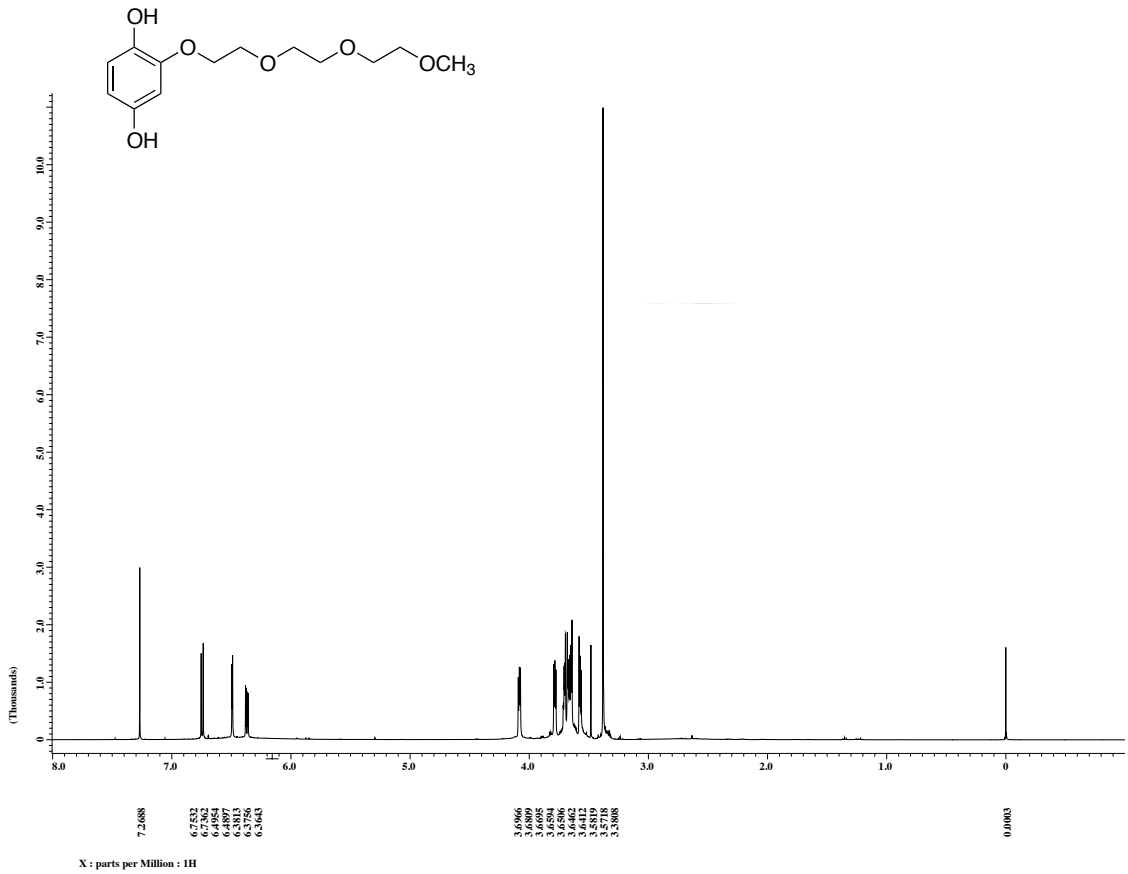

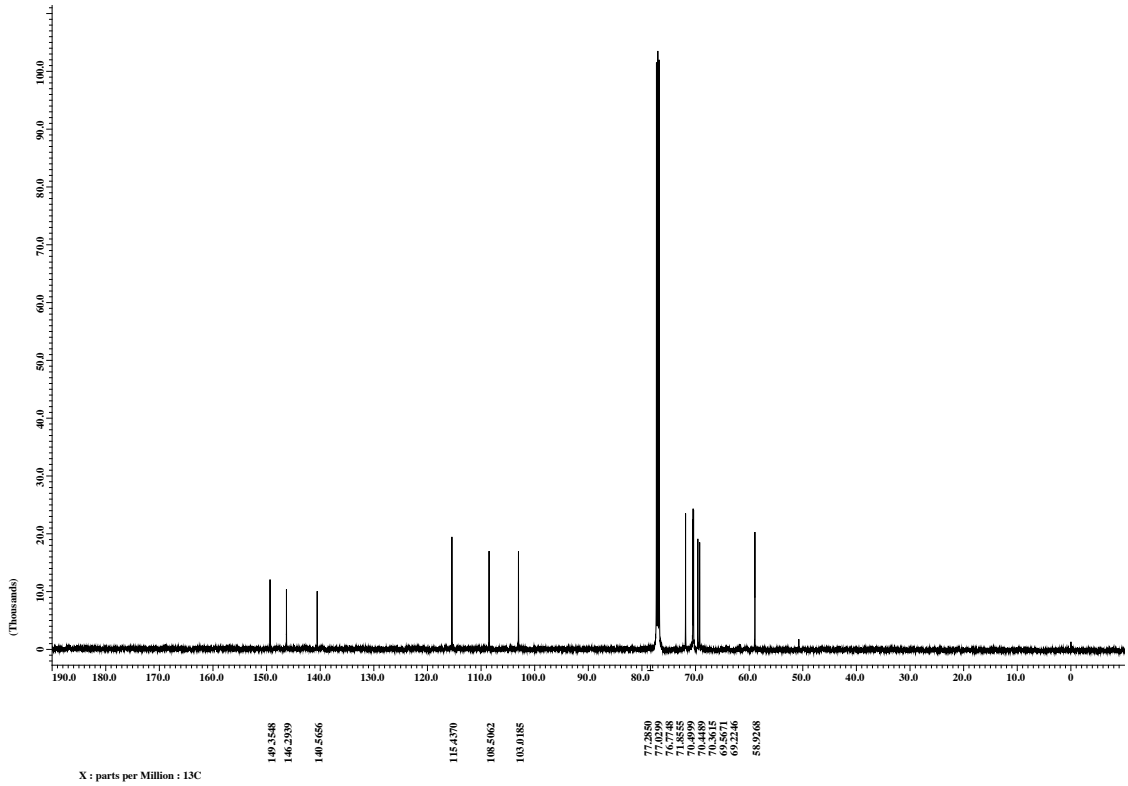

(h) ^{1}H and ^{13}C NMR spectra of **2aE$_3$** in $CDCl_3$

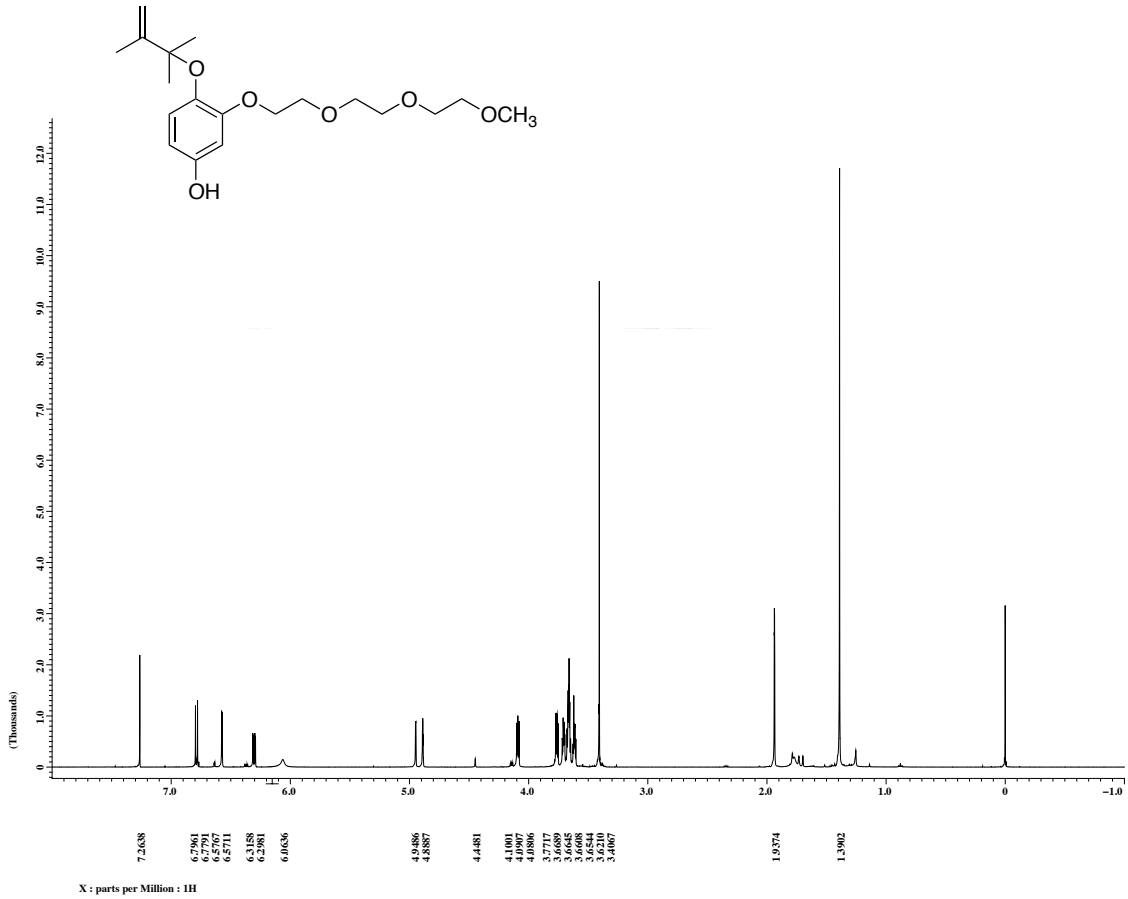

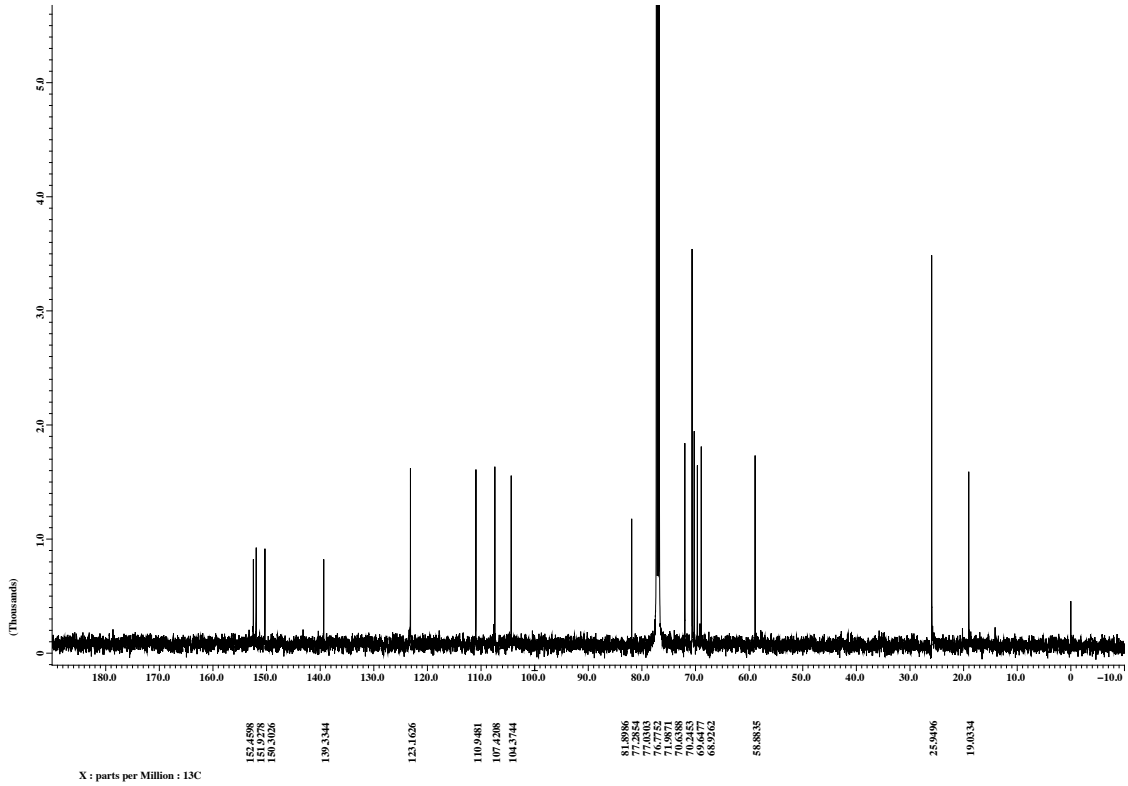

(i) ^{1}H and ^{13}C NMR spectra of **2bE$_3$** in $CDCl_3$

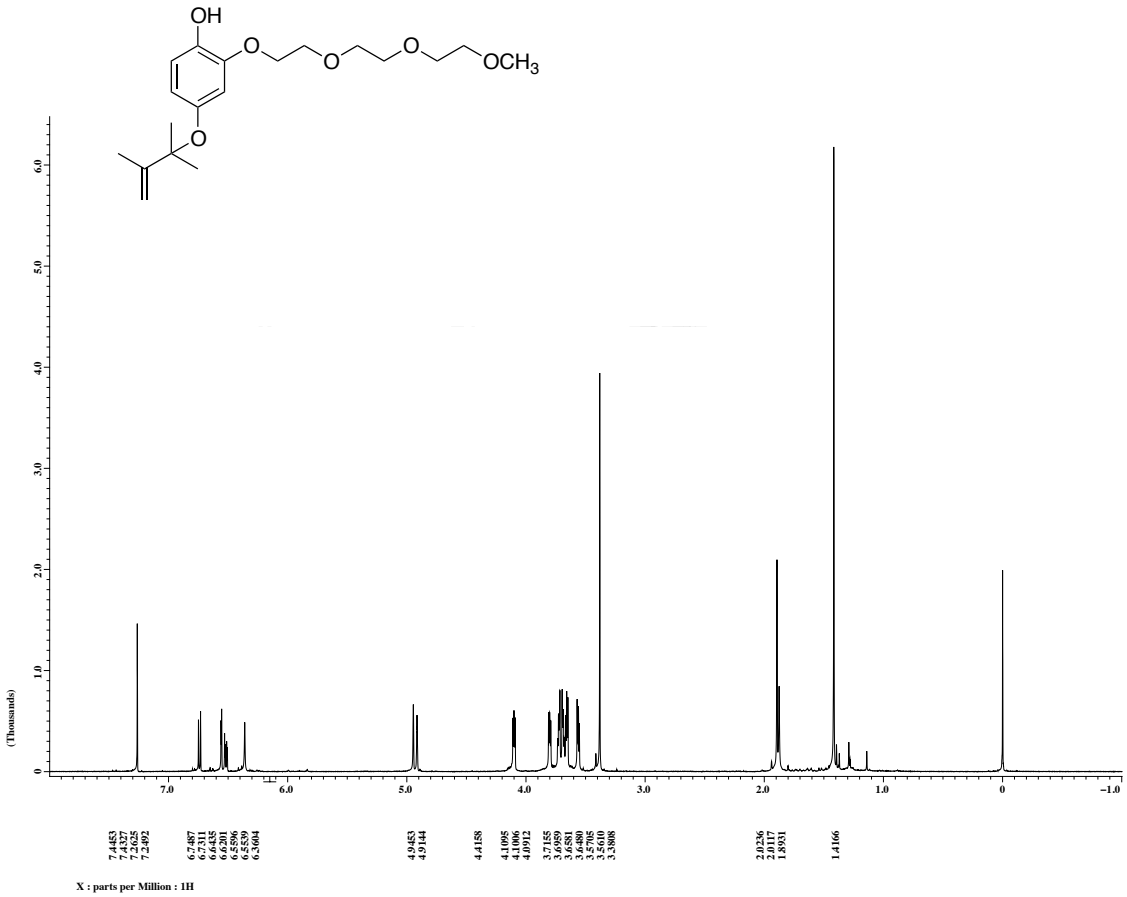

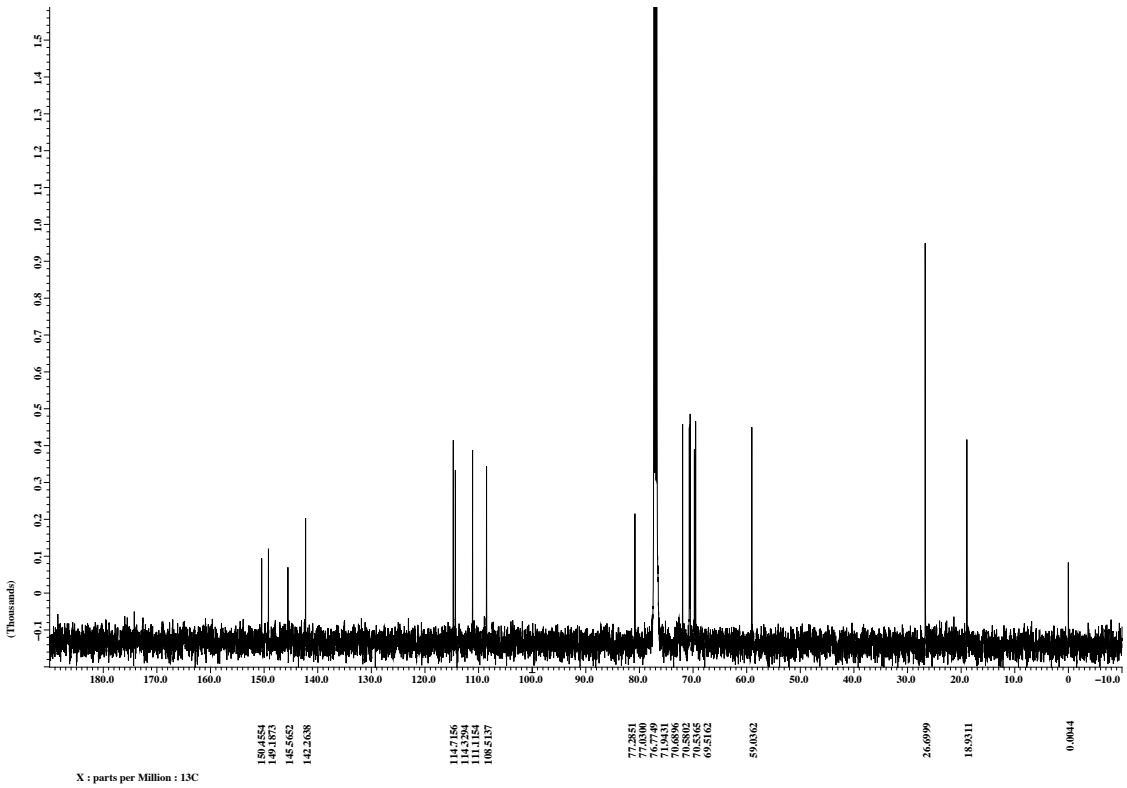

20. References

(1) T. Itoh and R. Hashimoto, *J. Lumin.*, 2012, **132**, 236.

(2) M. J. Frisch, G. W. Trucks, H. B. Schlegel, G. E. Scuseria, M. A. Robb, J. R. Cheeseman, G. Scalmani, V. Barone, B. Mennucci, G. A. Petersson, H. Nakatsuji, M. Caricato, X. Li, H. P. Hratchian, A. F. Izmaylov, J. Bloino, G. Zheng, J. L. Sonnenberg, M. Hada, M. Ehara, K. Toyota, R. Fukuda, J. Hasegawa, M. Ishida, T. Nakajima, Y. Honda, O. Kitao, H. Nakai, T. Vreven, J. A. Montgomery, Jr., J. E. Peralta, F. Ogliaro, M. Bearpark, J. J. Heyd, E. Brothers, K. N. Kudin, V. N. Staroverov, R. Kobayashi, J. Normand, K. Raghavachari, A. Rendell, J. C. Burant, S. S. Iyengar, J. Tomasi, M. Cossi, N. Rega, J. M. Millam, M. Klene, J. E. Knox, J. B. Cross, V. Bakken, C. Adamo, J. Jaramillo, R. Gomperts, R. E. Stratmann, O. Yazyev, A. J. Austin, R. Cammi, C. Pomelli, J. W. Ochterski, R. L. Martin, K. Morokuma, V. G. Zakrzewski, G. A. Voth, P. Salvador, J. J. Dannenberg, S. Dapprich, A. D. Daniels, Ö. Farkas, J. B. Foresman, J. V. Ortiz, J. Cioslowski and D. J. Fox, Gaussian 09, Revision A.1, Gaussian, Inc., Wallingford CT, 2009.

(3) Crystallographic data for the structure of **2aE$_0$** has been deposited with the Cambridge Crystallographic Data Center as supplementary publication numbers CCDC 894295.

(4) G. M. Sheldrick, SHELXTL 5.10 for Windows NT: Structure Determination Software Programs, Bruker Analytical X-ray Systems, Inc., Madison, WI, 1997.